Journal of the Meteorological Society of Japan, Vol. 92, No. 1, pp. 71−93, 2014
DOI:10.2151/jmsj.2014-105

An Intensification Process of a Winter Broad Cloud Band on a Flank of the Mountain Region along the Japan-Sea Coast

Tadayasu OHIGASHI, Kazuhisa TSUBOKI

Hydrospheric Atmospheric Research Center, Nagoya University, Nagoya, Japan

Yukari SHUSSE

National Research Institute for Earth Science and Disaster Prevention, Tsukuba, Japan

and

Hiroshi UYEDA

Hydrospheric Atmospheric Research Center, Nagoya University, Nagoya, Japan

(Manuscript received 29 November 2012, in final form 22 October 2013)

Abstract

During a cold-air outbreak between 25 and 27 January 2009, a broad cloud band formed along the coastal region from San-in to Hokuriku on the Sea of Japan side of the Japanese Islands. Along the mountain flank, precipitation in the cloud band was intensified. Intensification processes of the broad cloud band and microphysical characteristics of the intensified precipitation region were examined. During the lifetime of the cloud band, two low-pressure systems successively developed in the central Sea of Japan. Between the San-in and Hokuriku coastal regions located south of the low-pressure systems, westerly winds were predominant. It can be theoretically explained that the winds are blocked at least below 900 m by a high mountain region in Hokuriku. When the predominant westerly winds flowed into a high-pressure-gradient region produced by the blocking, unbalanced flow with ageostrophic winds formed. The relatively high pressure forced the westerly winds toward the left, resulting in southwesterly winds. The southwesterlies made a convergence with the predominant westerlies, the area of which corresponded to the intensified precipitation region. The correlation coefficient between vertical and horizontal polarized return signals (ρ_{hv}) averaged for 2 days indicates that melting particles were present below a height of several hundred meters in some periods and/or regions with surface temperature higher than 0°C. Above the melting level, the radar reflectivity (Z_h) maximum in the intensified precipitation region was more than or equal to 35 dBZ during one-third of the 2-day lifetime of the cloud band. For portions of $Z_h \geq 30$ dBZ, the mode of specific differential phase (K_{DP}) had negative values, which indicates the predominance of prolate graupel in the intensified precipitation region.

Keywords cloud band; cold-air outbreak; Sea of Japan; polarimetric radar; orographic effect; precipitation intensification

1. Introduction

In winter season, cold-air outbreaks frequently occur over seas and lakes to the west of extratropical cyclones. Heat and moisture are supplied to continental cold and dry air masses from relatively warm seas and

Corresponding author: Tadayasu Ohigashi, Hydrospheric Atmospheric Research Center, Nagoya University, Nagoya 464-8601, Japan
E-mail: ohigashi@rain.hyarc.nagoya-u.ac.jp

lakes, thus developing snow clouds. These clouds cause snowfall on the downwind side of seas and lakes. Snowfall is occasionally concentrated within a limited region, which results in heavy snowfall. Such a localized concentration is caused by mesoscale convective snowfall systems and local snowfall intensification. To understand the localized processes of snowfall, it is important to clarify the formation and development processes of mesoscale snowfall systems and their intensification processes.

Mesoscale snowfall systems associated with snowfall concentration have meso-α to meso-β scales (Orlanski 1975) and/or stagnant properties. Morphological characteristics are classified into vortical and linear shapes. A polar low is a mesoscale cyclone forming on the poleward side of the main baroclinic zone (e.g., Rasmussen and Turner 2003), and is identified as a vortical system causing snowfall concentration. The formation and development of polar lows are strongly affected by baroclinicity, convective activity (e.g., Yanase and Niino 2007), and mid-tropospheric cold lows (e.g., Ninomiya 1989; Rasmussen and Turner 2003).

Linear-shaped snowfall systems associated with snowfall concentration develop as broad cloud bands (e.g., Hjelmfelt 1990; Niziol et al. 1995; Grim et al. 2004; Kawase e t al. 2005; Maesaka et al. 2006). These bands have wider horizontal scales than cloud streets (e.g., Kuettner 1959, 1971; Brown 1980; Etling and Brown 1993; Atkinson and Zhang 1996; Young et al. 2002; Fujiyoshi et al. 1998; Renfrew and Moore 1999; Yoshimoto et al. 2000; Liu et al. 2004; Yamada et al. 2010), commonly developing during cold-air outbreaks. Formation processes of the broad cloud bands are strongly connected with orography and surface conditions. Therefore, most broad cloud bands form in specific locations. Over the Sea of Japan, the broadest cloud bands form along a convergence zone in the western part of the sea (Okabayashi 1969; Yagi et al. 1986; Nagata et al. 1986; Nagata 1987, 1991, 1992; Ohigashi and Tsuboki 2007; Eito et al. 2010; Ohigashi et al. 2012). The convergence zone generating the broadest cloud bands is referred to as the Japan-Sea Polar-Airmass Convergence Zone (JPCZ) (Asai 1988). In this study, cloud bands along JPCZ are referred to as the JPCZ cloud bands. Other broad cloud bands also form on the lee side of the Sikhote-Alin mountain range on the east coast of the Eurasian continent (Muramatsu 1979; Ohtake et al. 2009), off the western coast of Hokkaido (Fig. 1a) (Fujiyoshi et al. 1988; Tsuboki et al. 1989a; Sasaki and Satomura 1991), to the lee of a mountain in western Hokkaido (Fujiyoshi et al. 1992), and along the northeast coast of Hokkaido (Fujiyoshi et al. 2009).

These convective snowfall clouds can be intensified via certain processes. Nagata (1992) and Ohigashi and Tsuboki (2007) showed that the JPCZ cloud bands intensified under upper-level mesoscale cold lows. Takeda et al. (1982) showed the intensification of isolated snow clouds near a coast. They explained that intensification began as a result of variation in vertical shear of the prevailing wind near the land. Eito et al. (2005) showed that a cold pool beneath a snowband significantly contributed to the formation of convection. They indicated that the cold pool was caused by diabatic cooling from the sublimation of snow. Ookubo and Kurokawa (2000) and Yoshihara et al. (2004) mentioned that winds were locally deflected by mountains. This deflection produced convergence with surrounding winds and intensified precipitation. However, the dynamics of such deflections was not shown.

Snowfall intensification at land-breeze fronts in coastal regions have been reported (Passarelli and Braham 1981; Ishihara et al. 1989; Tsuboki et al. 1989b; Laird et al. 2003; Ohigashi and Tsuboki 2005). Ohigashi and Tsuboki (2005) inferred particle types of precipitation in a snowfall intensification region at a land-breeze front using a C-band polarimetric radar, and discussed predominant microphysical processes. They used polarimetric parameters of radar reflectivity and differential reflectivity, and demonstrated that graupel was predominant at the land-breeze front, and snow aggregates behind it. This resulted in double peaks of reflectivity. Understanding particle types such as snow aggregates and graupel are important for estimating precipitation intensity and amount, and for inferring cloud microphysical processes. Polarimetric radar is a powerful tool for estimating spatial distributions of particle types. In snowfall intensification regions of stronger precipitation intensity during cold-air outbreaks, however, characteristics of other polarimetric parameters and their effectiveness in identifying particle types have not been examined.

Between 25 and 27 January 2009, a broad cloud band formed along the northern coastal region of the western Japanese Islands. A convergence line located at the same position as this cloud band has been noticed in the previous studies (Katsutani 1947; Ino 1965; Japan Meteorological Agency 1968). The broad cloud band showed continuous and distinct intensifications of snowfall along the mountain flank, thus generating heavy snowfall. The main objective is to clarify dynamical processes inducing snowfall

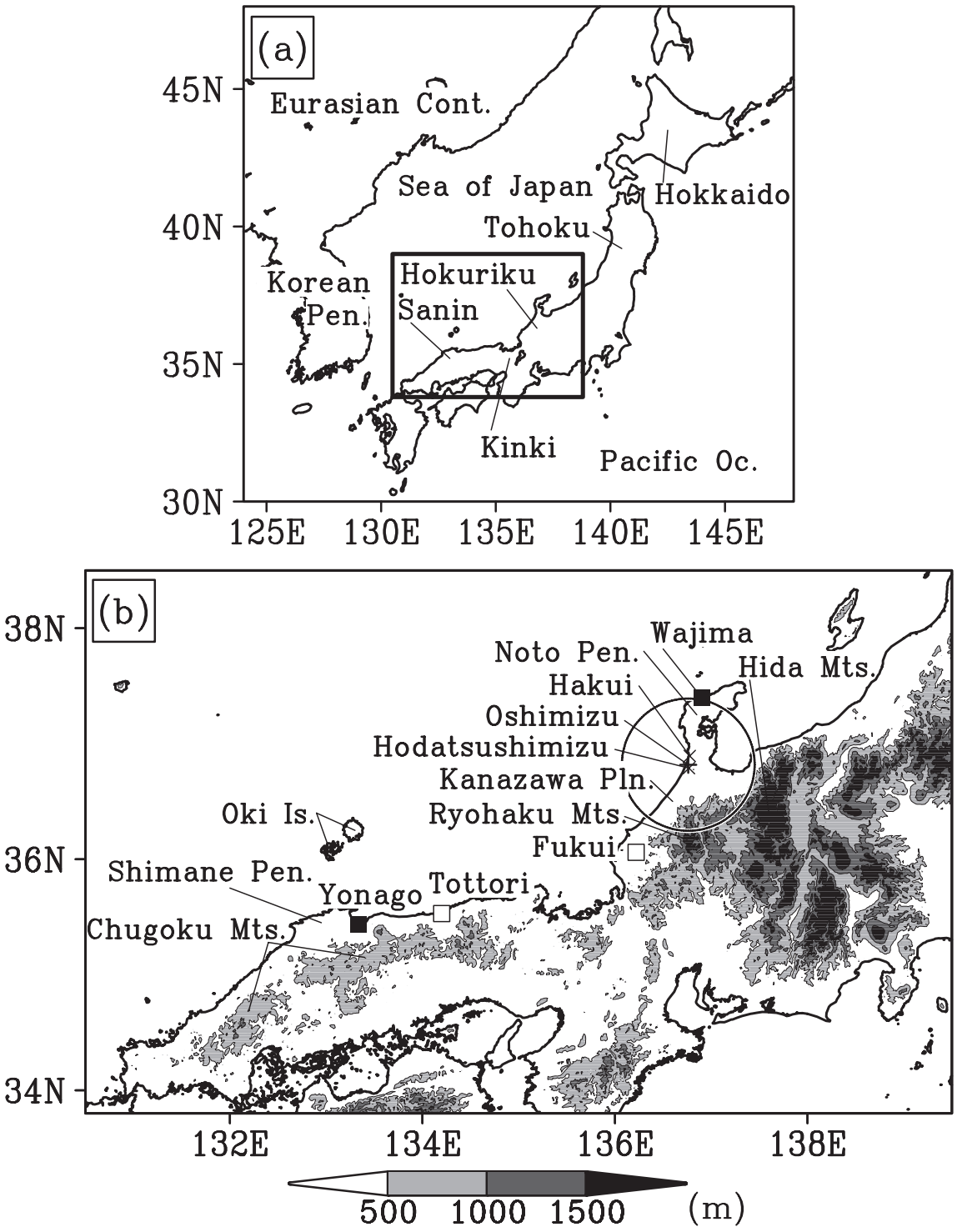

Fig. 1. Locations of observation points. (a) Map of the Sea of Japan region. (b) Close-up view of square region in Fig. 1a. Gray levels show the altitude of topography (m). The plus symbol and surrounding large open circle indicate the observation site and range of Nagoya University polarimetric radar, respectively. Closed and open squares show upper-air sounding observation sites and wind profilers, respectively. Crosses show AMeDAS surface observation sites.

intensification along the mountain flank. In addition, the characteristics of multiple polarimetric parameters are examined to show predominant particle types associated with regional precipitation intensity. The locations of several geographical names, which appear in the following text, are summarized in Fig. 1.

2. Observation and data

A Nagoya University polarimetric radar was deployed at Oshimizu in Hokuriku (36°49′17″N, 136°45′31″E, 26 m; Fig. 1b) from 20 December 2008, to 12 March 2009. The radar transmitting frequency is 9375 MHz (X band). The radar has two separate transmitters with solid-state elements for power amplification. Polarized waves were transmitted at 45° to the ground surface. Although the peak transmitting power is 200 W, a chirp-type pulse compression technique is used for 29.1 μs pulse to achieve large signal power. Within a distance of 4.8 km from the radar, data could not be acquired using this long pulse. Therefore, data obtained from 4.8 to 61.8 km from the radar were available for analysis. The range gate and beam widths were 150 m and 1.2°, respectively. Pulse repetition frequencies were switched for every ray between 1600 and 2000 Hz. The available polarimetric parameters were equivalent radar reflectivity obtained by horizontally polarized waves (Z_h), differential reflectivity (Z_{DR}), differential phase (Φ_{DP}), and correlation coefficient (ρ_{hv}). After small-scale variabilities of Φ_{DP} were removed by a filter, specific differential phase (K_{DP}) was derived from least-square fitting of divisional Φ_{DP}. No attenuation correction was used for Z_h and Z_{DR}. ρ_{hv} with noise (observed value) is smaller than that without noise (true value) as a function of signal-to-noise ratio, which is a measure indicating the level of a desired signal to that of background noise. Therefore, a correction using signal-to-noise ratio was applied to observed ρ_{hv} (Schuur et al. 2003; Shusse et al. 2009). The radar was operated with 12 plan position indicator (PPI) scans at elevation angles from 0.6° to 20° in 5 min. Some additional specifications are shown in Morotomi et al. (2012).

Upper-air sounding (0900 JST and 2100 JST (9 h ahead of UTC)) and wind profiler data (every 10 min) obtained from routine observations of the Japan Meteorological Agency (JMA) were used for examining the upper-air environment. In addition, 1-hourly surface atmospheric data from the Automated Meteorological Data Acquisition System (AMeDAS) of the JMA, composite radar precipitation intensity data every 10 min at a height of 2 km from operational JMA radars, 1-hourly precipitation amount distributions estimated by the JMA, and geostationary meteorological satellite data were used to examine the cloud and precipitation distribution and the environment near intensified precipitation regions. Precipitation amount distributions estimated by the JMA were radar-estimated precipitation amounts that were calibrated by AMeDAS rainfall gauges. To examine synoptic-scale and mesoscale environments, we used 6-hourly available JMA Climate Data Assimilation System (JCDAS) reanalysis with a horizontal resolution of 1.25°, and 3-hourly available JMA mesoscale objective analysis (MA) with a horizontal resolution of 10 km. The JCDAS reanalysis procedure is the same as that of the Japanese 25-year reanalysis (Onogi et al. 2007).

3. Overview of the broad cloud band

Figure 2 shows an infrared image of a geostationary meteorological satellite at 0600 JST 25 January 2009. The satellite image shows a cloud band formed near the coastline from the Shimane Peninsula to the Noto Peninsula, which is shown by a dashed ellipse in Fig. 2. The broad cloud band targeted in this study stagnated at almost the same position, while internal snow clouds moved along the band. The target cloud band is very broad relative to other cloud streets developing over the Sea of Japan, and is different from the JPCZ cloud bands, which are known as major broad cloud bands developing over the Sea of Japan.

The position of the target cloud band is shown in a time-latitude cross-section of JMA radar-estimated precipitation intensity along the line A0–A1 in Fig. 2, every 10 min between 0000 JST 24 January and 2100 JST 27 January (Fig. 3). Precipitation intensity in excess of 1 mm hr^{-1}, which is associated with the target cloud band, is continuously present between 36.3°N and 37.2°N. The cloud band is located at nearly the same position after 0300 JST 25 January, except at around 0300 JST 26 January, at which time it moved northward. After 0300 JST 27 January, the precipitation intensity weakened. Therefore, the period between 0300 JST 25 January and 0300 JST 27 January is focused hereafter.

Figure 4 shows the precipitation amounts between 0300 JST 25 January and 0300 JST 27 January, when the broad cloud band almost stagnated, obtained by integrating 1-hourly precipitation amounts estimated by the JMA. A band of large precipitation amounts, more than 20 mm, extends from the Shimane Peninsula to the Noto Peninsula. In the band, two precipitation maxima are found. One is off the San-in and Kinki coastal regions, with precipitation amounts greater than 40 mm. The other is over the Noto Peninsula,

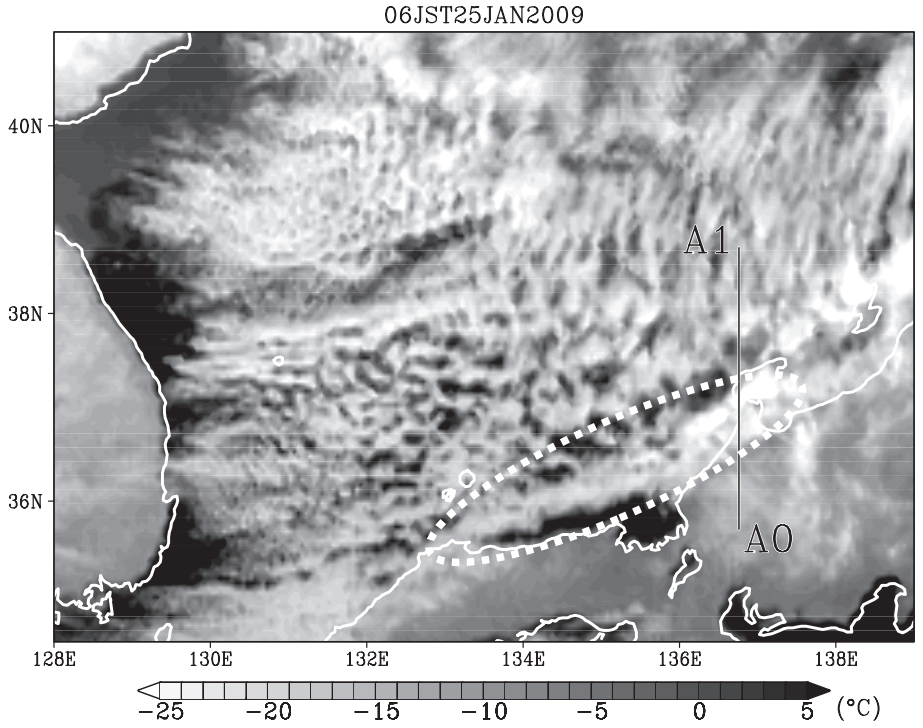

Fig. 2. Meteorological satellite infrared image at 0600 JST 25 January 2009. Gray scale shows brightness temperature (°C). Dashed ellipse indicates the target broad cloud band in this study.

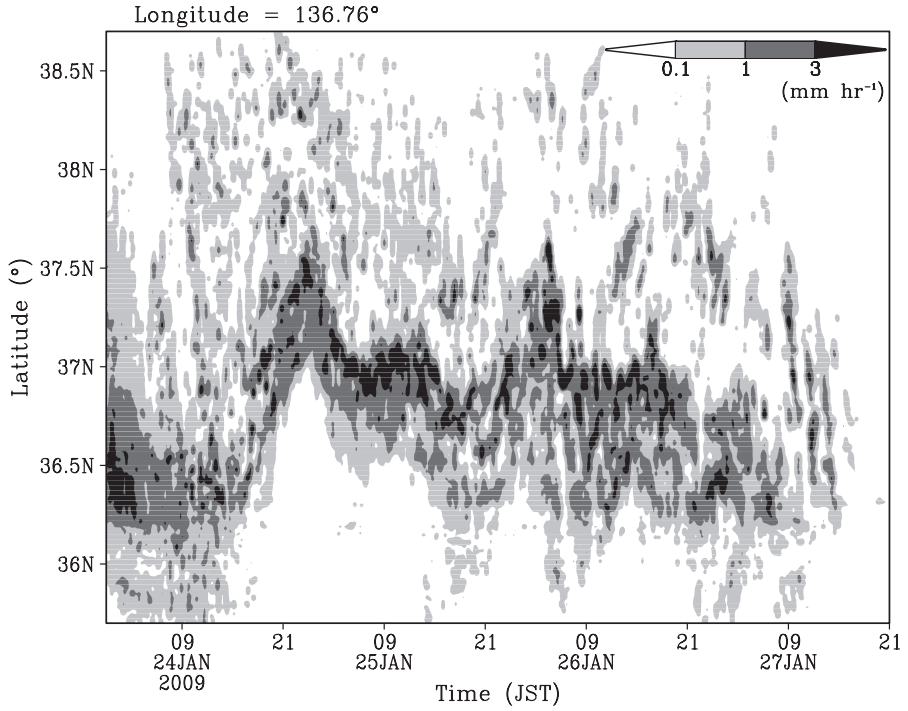

Fig. 3. Time-latitude cross-section of JMA radar precipitation intensity (mm h^{-1}) between 0000 JST 24 January 2009 and 2100 JST 27 January 2009 along the line A0–A1 in Fig. 2.

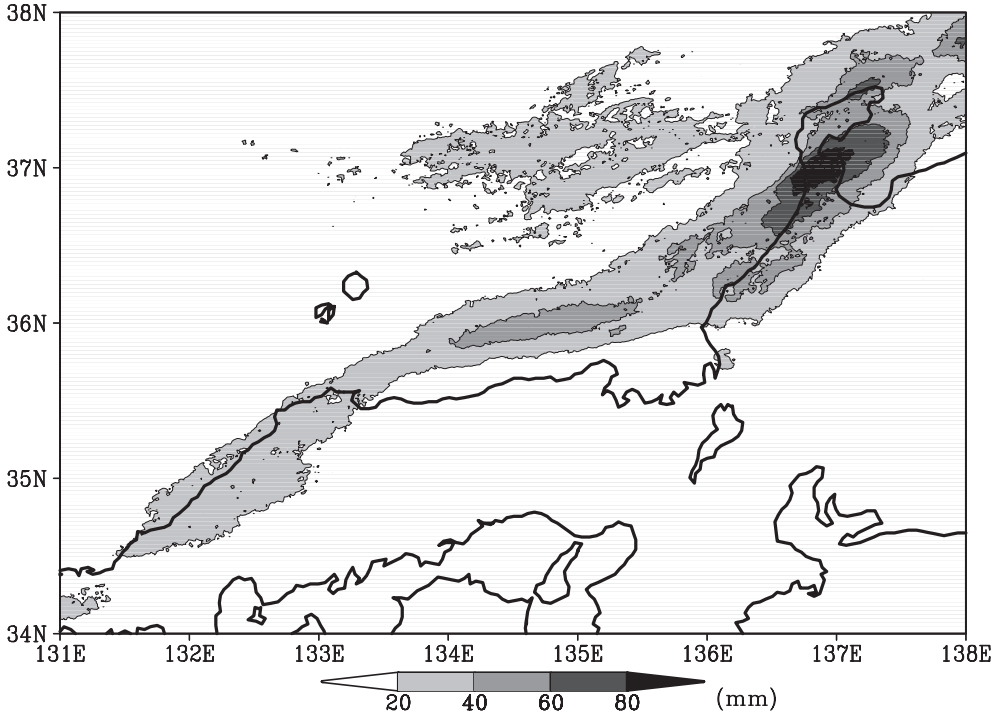

Fig. 4. Precipitation amount (mm) integrated for 48 h before 0300 JST 27 January 2009. The amount was estimated by radar-based precipitation intensity calibrated by surface rainfall gauges of the Japan Meteorological Agency. Contours are drawn every 20 mm.

with amounts more than 80 mm. Precipitation amounts of 95.5 mm at Hakui and 75.5 mm at Hodatsushimizu were observed by the AMeDAS rainfall gauges during the same period. The maximum amount on the Noto Peninsula was significantly larger than those in other parts of the broad cloud band. This indicates that the target cloud band is especially intensified around the location of precipitation maximum. We examine the process where strong precipitation (snowfall) is formed over the Noto Peninsula.

4. Local snowfall intensification processes

Behind a synoptic-scale low located east of the Japanese Islands, a cold air outbreak had already occurred on 24 January, 2009, over the Sea of Japan. Sea-level pressure and surface wind fields are shown in Fig. 5. Within the cold-air outbreak environment, a new low pressure formed over the Sea of Japan near the Eurasian continent at 2100 JST 24 January 2009 (A in Fig. 5a). South of the low pressure, westerly winds formed off the coast between the San-in and Hokuriku regions. The westerly winds were maintained even after the low pressure moved northeast (Fig. 5b). At 2100 JST 25 January, another low pressure (B in Fig. 5c) formed over the Sea of Japan, and the westerlies were maintained south of and behind the low-pressure center until the next day (Figs. 5c and 5d). A weak surface trough (thick dashed line in Fig. 5d) was seen behind low pressure B at 0900 JST 26 January. At 2100 JST 26 January, the northerly component slightly increased and the wind direction became west-northwesterly off the coast between the San-in and Hokuriku regions. The weak trough in the central Sea of Japan disappeared by 0900 JST 27 January, and the predominant wind direction changed to northwesterly. This change in the wind direction to more northerly almost corresponds to a dissipation of precipitation associated with the broad cloud band (Fig. 3).

To examine atmospheric stratification, vertical profiles of potential temperature, equivalent potential temperature and saturation equivalent potential temperature from an upper-air sounding observation at Wajima at 0900 JST 25 January are shown in Fig. 6a. A strong stable layer is present above 4000 m. Below this layer, a convective mixing layer with relatively small stability develops. This stratification is a common

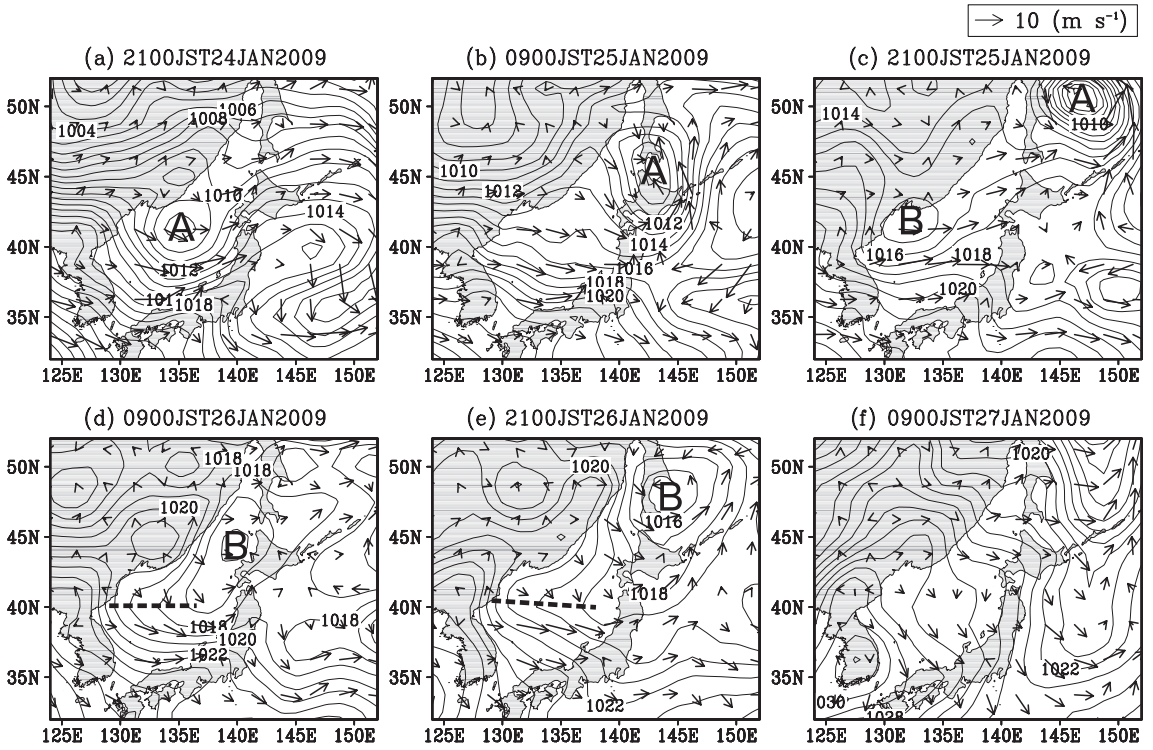

Fig. 5. Sea-level pressure (contours, hPa) and surface wind field (vectors, m s^{-1}) every 12 h between 2100 JST 24 January 2009 and 0900 JST 27 January 2009, depicted from the JCDAS. Broken lines and symbols A and B indicate a surface-pressure trough and low-pressure centers, respectively (see text for details).

feature around Hokuriku during cold-air outbreaks. The Brunt-Väisälä frequency $N = \{(g/\theta_v(z))(\partial\theta_v(z)/\partial z)\}^{1/2}$, where g is the gravitational acceleration and θ_v is the virtual potential temperature between the surface and 4000 m is 8.7×10^{-3} s^{-1}. The wind speed (Fig. 6b) increases with height. This increase is particularly notable below 1 km. Compared with stratification and wind speed at Yonago and those at other times at Wajima on 25 and 26 January, the stratification at 0900 JST 25 January below 2000 m at Wajima is comparable or less stable and wind speed is comparable or larger. This indicates that around Wajima at 0900 JST 25 January, low-level air flows were the most difficult to be blocked by mountains, which is explained using non-dimensional mountain height ($\hat{h}$) in the following.

To examine whether air flows over or around the topography, $\hat{h}$ is calculated for the Ryohaku Mountains, located downwind of the low-level westerlies (Fig. 1b). $\hat{h}$ is the inverse of the mountain Froude number (e.g., Markowski and Richarddon 2010) and is calculated as

$$\hat{h}(z) = \frac{N(z) \cdot (h_m - z)}{U(z)} \quad (1)$$

where $N(z)$ is the average Brunt-Väisälä frequency between height z and mountain height h_m, and $U(z)$ is the wind speed at height z. $\hat{h}$ is a measure of whether an air parcel with wind speed $U(z)$ at height z flows over or around the topography. $\hat{h}$ greater than unity indicates that an air parcel will be blocked by mountains. Figure 7 shows the vertical profiles of $\hat{h}$ obtained from the upper-air sounding data at Wajima at 0900 JST 25 January. For h_m, we used the altitude of Mt. Hakusan (2702 m), which is the highest peak in the Ryohaku Mountains. The range of $z > h_m$, where $\hat{h}$ is negative, is not shown because it is obvious that the air parcel flows over the topography. $\hat{h}$ ordinarily increases toward the surface mainly due to the extension of the distance between h_m and z toward the surface. In addition, $U(z)$ decreases notably near the surface (Fig. 6b), which results in large $\hat{h}$ near the surface. The height where $\hat{h}$ equals unity is 920 m (Table 1), which indicates that an air parcel will be blocked by the Ryohaku Moun-

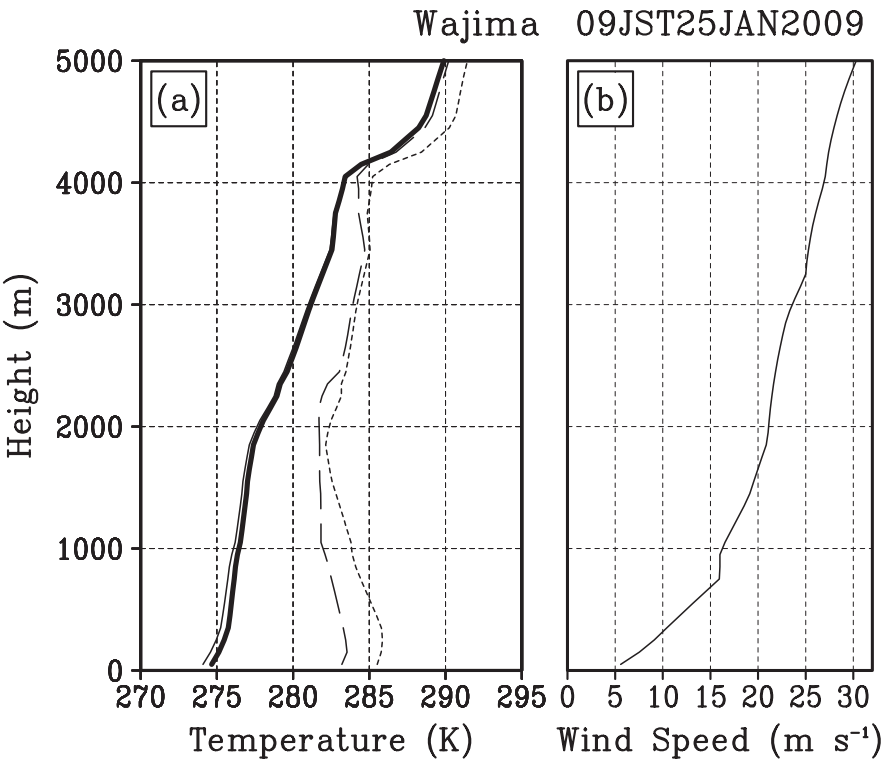

Fig. 6. Upper-air sounding profile at 0900 JST 25 January 2009 at Wajima. (a) Potential temperature (thin solid line, K), equivalent potential temperature (broken line, K), saturation equivalent potential temperature (dashed line, K), and virtual potential temperature (thick solid line, K); and (b) wind speed (m s^{-1}).

tains below this height. At Wajima at other times on 25 and 26 January and at Yonago on 25 and 26 January, critical heights where values of $\hat{h}$ equaled unity were between 940 and 1280 m and between 1270 and 1730 m, respectively (Table 1). This indicates that air parcels at least below 900 m were blocked by the Ryohaku Mountains when the target cloud band stagnated.

Local wind patterns and directional constancy (*DC*) (e.g., Bromwich 1989) in the surrounding westerly winds for 48 h prior to 0300 JST 27 January are shown in Fig. 8. The barbs and gray scale indicate vector-average winds and *DC*, respectively, derived from the AMeDAS surface wind data. *DC* is defined as the ratio of the magnitude of vector-averaged wind to the averaged scalar wind speed:

$$DC = \frac{|\overline{\mathbf{v}}|}{\overline{|\mathbf{v}|}} = \frac{\sqrt{\left(\frac{1}{n}\sum_{i=1}^{n} u_i\right)^2 + \left(\frac{1}{n}\sum_{i=1}^{n} v_i\right)^2}}{\frac{1}{n}\sum_{i=1}^{n}\sqrt{u_i^2 + v_i^2}} \qquad (2)$$

where **v** is the horizontal wind vector, overbars indicate time average, u and v are zonal and meridional components of the wind velocity, respectively and n is the number of data. *DC* has a value between zero and unity. As DC is closer to unity, the mind direction is less changed during a period. In the Oki Islands in the Sea of Japan (Fig. 1b), vector-averaged winds are westerlies and *DC*s are above 0.9. The wind direction agrees with the surface wind direction off the coast between the San-in and Kinki regions (Fig. 5). Therefore, the wind direction at the Oki Islands represents the predominant winds off the coast between the San-in and Kinki regions during the period. On the other hand, average winds are southwesterly in coastal portions of the San-in and Kinki regions, located south of the target broad cloud band. *DC*s in wide areas of those regions are less than 0.8, with a few exceptions. A high *DC* area, with a value greater than 0.9, extends from the Kanazawa Plain to the Noto Peninsula. Over the plain, south of the broad cloud band, the wind direction is approximately south-southwesterly. Over the northern Noto Peninsula, north of the cloud band, southwesterly winds blow, except the westernmost point, which

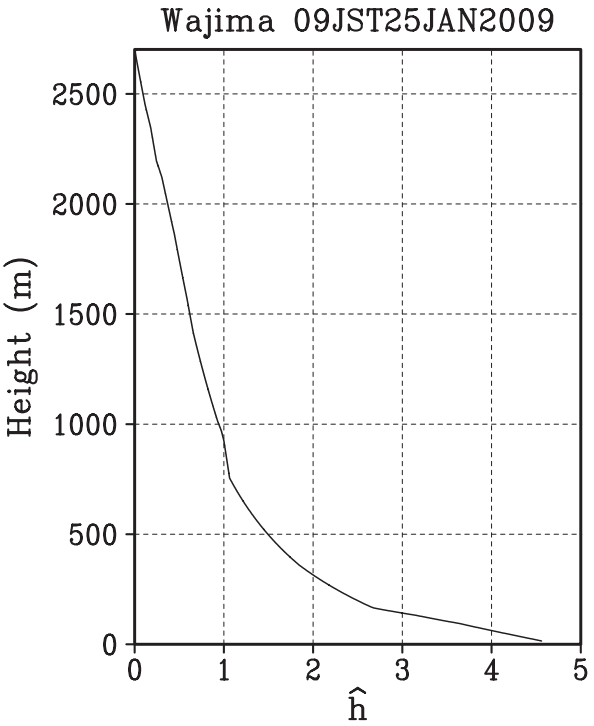

Fig. 7. Vertical distribution of non-dimensional mountain height ($\hat{h}$) derived from an upper-air sounding observation at 0900 JST 25 January 2009 at Wajima.

is located on the upwind side of the cloud band. High *DC* indicates that these wind directions with southerly component were maintained, while westerly winds were predominant in the upwind region of the cloud band. This high *DC* area is located to the northwest of the Ryohaku Mountains.

Figures 9a and 9b show temporal changes of vertical distributions of horizontal winds observed by wind profilers at Tottori and Fukui, respectively. Fukui is located immediately upwind of the Ryohaku Mountains. Although Tottori is also located upwind, the distance is so long that the winds at Tottori are unaffected by the Ryohaku Mountains. During the persistence of the target cloud band between 0300 JST 25 January and 0300 JST 27 January, westerly winds are predominant above 2500 m at both sites. However, wind directions below this height are different. At Tottori, wind directions at the lowest level (414 m) are roughly southwest, and winds with a large southerly component (wind direction: 135°–225°) are almost limited below the second level (710 m), except at around 1800 JST 25 January. On the other hand, directions at Fukui are

Table 1. Heights (m) where values of non-dimensional mountain height $\hat{h}$ equal unity. Upper-air sounding observation data at Wajima in January 2009 were used.

Time	Wajima	Yonago
0900 JST, 25	920	1350
2100 JST, 25	1280	1270
0900 JST, 26	1080	1500
2100 JST, 26	940	1730

approximately southerly at the lowest level (403 m) and winds with the large southerly component extend up to 1500–2000 m. This indicates that the blocking effect of the Ryohaku Mountains on the westerlies was important for developing the southerly component at the low level in the immediately upwind area.

Horizontal wind divergence (convergence) around the cloud band at the low level is estimated by the MA data. Figure 10 shows horizontal divergence and horizontal wind fields at 950 hPa, averaged between 0300 JST 25 January and 0300 JST 27 January. The westerly winds over the sea and west-southwesterly winds near the coast forms a convergence line of stronger than -0.5×10^{-4} s^{-1} offshore between San-in and Hokuriku. This low-level convergence line is collocated with the target broad cloud band (Fig. 2). Around the high *DC* area in AMeDAS surface data along the flank of the Ryohaku Mountains, the wind direction shifts from westerly on the upwind side to southwesterly, which is consistent with the surface winds shown in Fig. 8. The shift produces low-level convergence stronger than -1.5×10^{-4} s^{-1} to the west of Hokuriku. The strong convergence area coincided with the snowfall intensification region on the Noto Peninsula (Fig. 4). Therefore, the production of southerly component in predominant westerlies on the upwind side was important for the snowfall intensification.

To study the formation of the southerly component, geopotential heights and magnitudes of the pressure gradient force at 950 hPa averaged between 0300 JST 25 January and 0300 JST 27 January are shown in Fig. 11. Over the sea east of 134.5°E, isolines of geopotential heights are almost aligned in an east–west direction. This is consistent with the predominant westerly winds. Upwind of the Ryohaku Mountains, the geopotential height contours are densely packed, which produces locally high magnitudes of pressure gradient force.

Neglecting turbulent mixing, the horizontal momentum equation is as follows:

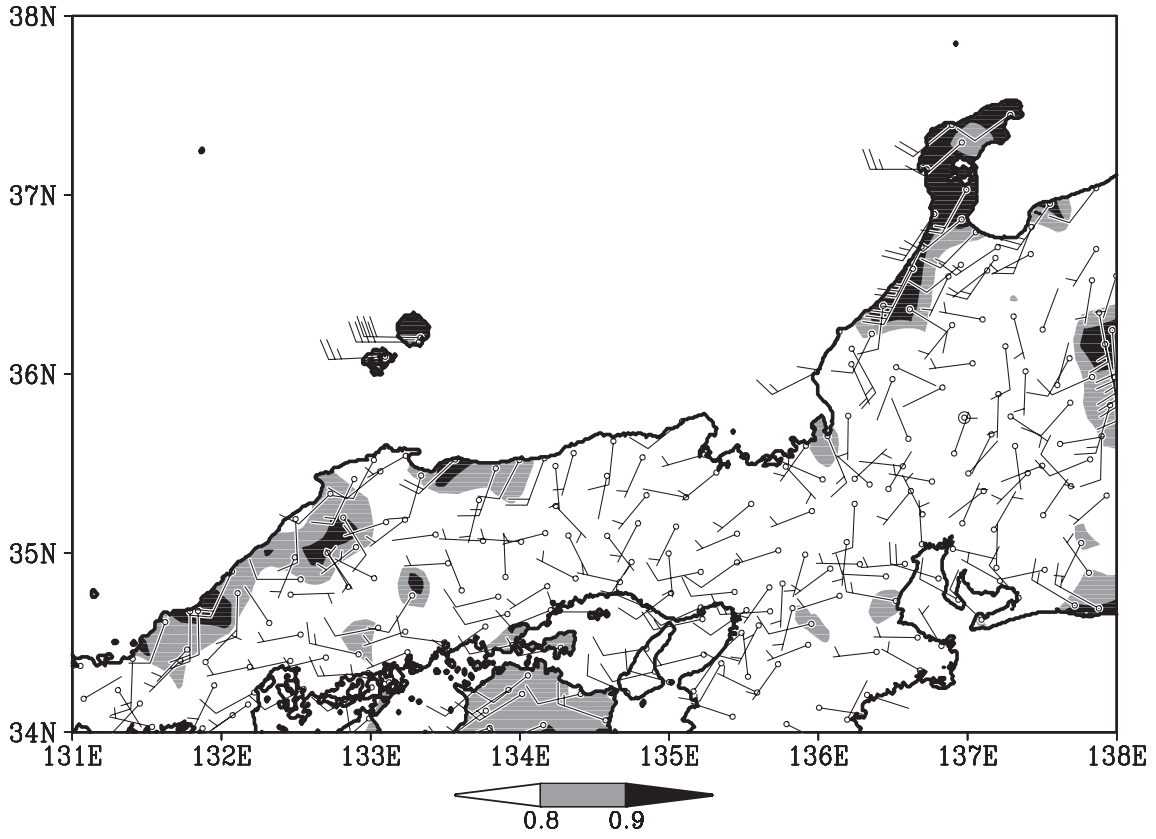

Fig. 8. Surface wind fields (barbs, m s^{-1}) averaged for 48 h prior to 0300 JST 27 January 2009, and directional constancy (gray scale). Double open circles, half barbs, and full barbs indicate cases of calm wind, 1 m s^{-1} speed wind, and 2 m s^{-1}, respectively.

$$\frac{d\mathbf{v}}{dt} = -\nabla\Phi - f\,\mathbf{k}\times\mathbf{v} = \underbrace{-f\,\mathrm{k}\times\mathbf{v_a}}_{F_{ageo}} \tag{3}$$

where Φ is geopotential, f is the Coriolis parameter, $\mathbf{k}$ is the unit vector in the vertical direction, and $\mathbf{v_a}$ is the ageostrophic wind vector. This indicates that temporal change of the horizontal velocity depends on a force balance between the pressure gradient and Coriolis forces, which is the Coriolis force working on the ageostrophic wind $\mathbf{v_a}$ (F_{ageo}). Figure 12 shows the ageostrophic wind vector and its magnitude. Over the sea, ageostrophic wind speed is small, which means that the horizontal winds are nearly in geostrophic balance. In the adjacent sea area upwind of the Ryohaku Mountains, ageostrophic wind vectors are directed to the west, opposite to the predominant westerly wind direction over the sea. This indicates that wind speeds with large ageostrophic components in this region are slower than the geostrophic wind speed.

F_{ageo} around the Ryohaku Mountains is shown in Fig. 13. A northward F_{ageo} is found on the upwind side of the Ryohaku Mountains. Following the flow south of the target cloud band, the westerly wind direction shifts to the left, which results in southwesterlies near the topography. This causes the area with convergence stronger than -1.5×10^{-4} s^{-1}. The leftward deflection of the westerlies is smaller far north of the mountains, which causes weaker convergence from the north portion of the Noto Peninsula to the sea. Therefore, a single convergence maximum forms to the north of the winds with a large southerly component. This convergence maximum causes the snowfall enhancement. The precipitation maximum area shown in Fig. 4 is found slightly leeward of the convergence maximum. This was caused by the leeward advection of precipitation particles from the region with updraft maximum.

5. Characteristics of polarimetric parameters

To clarify the microphysical characteristics in the vicinity of the wind convergence maximum along the

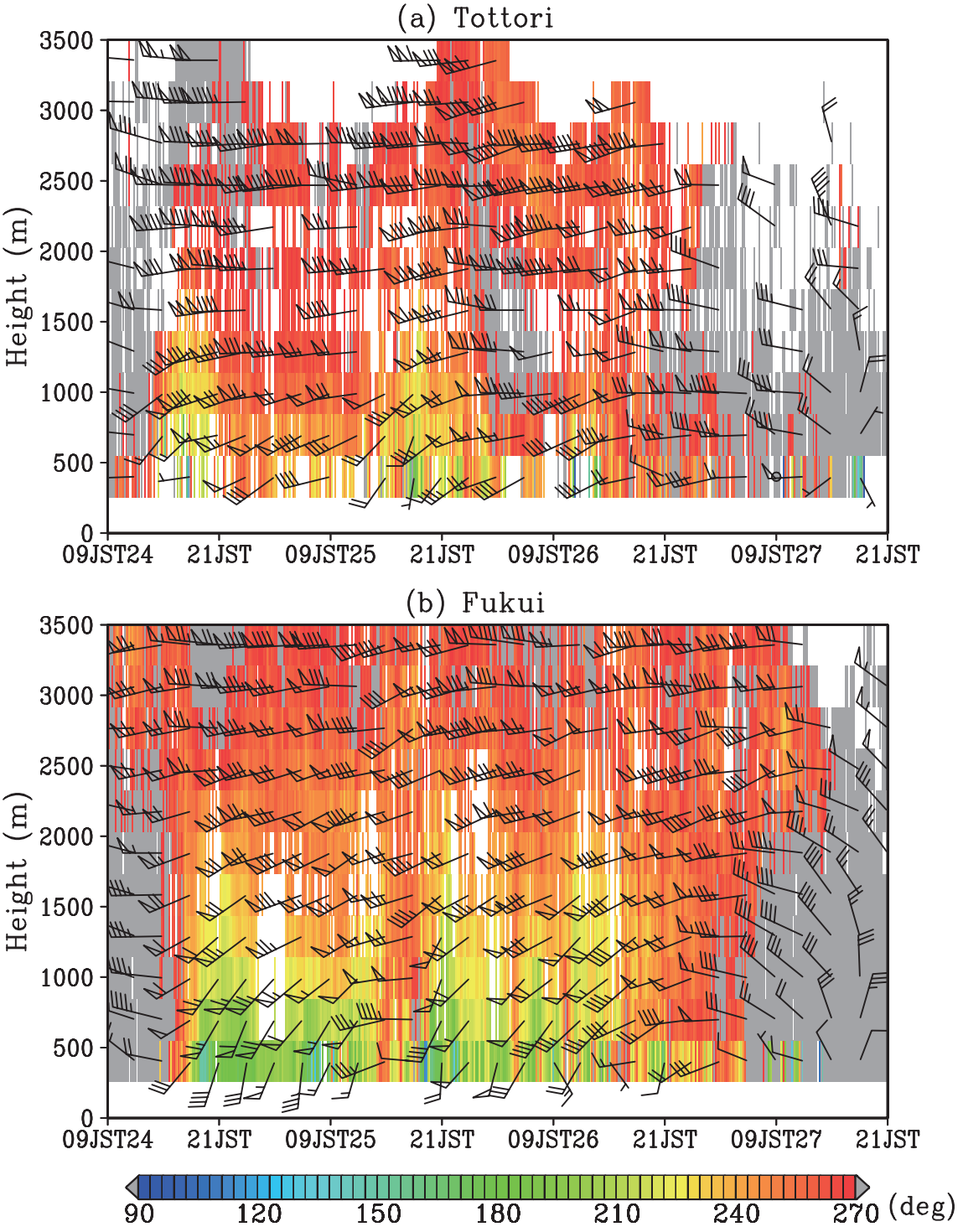

Fig. 9. Time-height cross-section of horizontal winds (barbs, m s^{-1}) obtained by wind profilers at (a) Tottori and (b) Fukui. Half barbs, full barbs, and flags show 1 m s^{-1}, 2 m s^{-1}, and 10 m s^{-1}, respectively. Color scales indicate the wind direction (°).

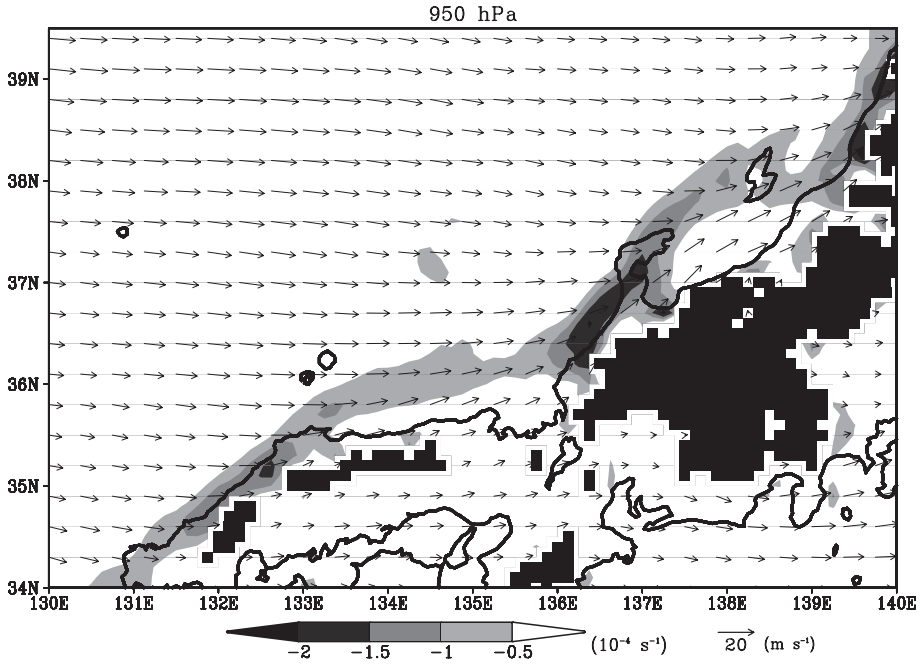

Fig. 10. Horizontal divergence (gray scale, 10^{-4} s^{-1}) and horizontal wind (vectors, m s^{-1}) fields at 950 hPa, depicted from the MA. All fields were averaged between 0300 JST 25 January 2009 and 0300 JST 27 January 2009. Areas below ground at 950 hPa are shaded black.

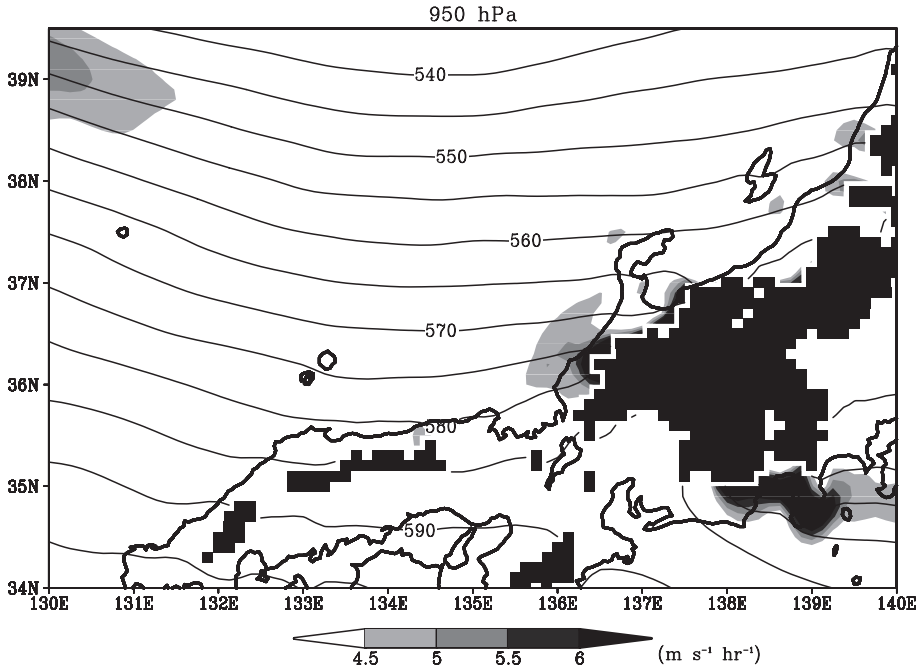

Fig. 11. Same as Fig. 10, except for geopotential height (contours, m) and magnitude of pressure gradient force (gray scale, m s^{-1} h^{-1}).

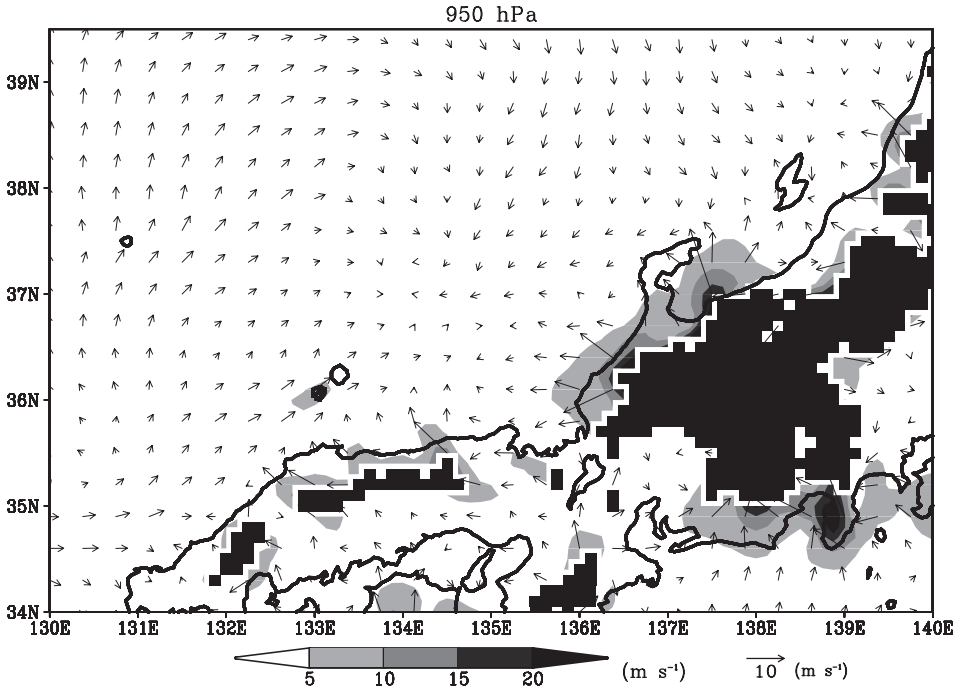

Fig. 12. Same as Fig. 10, except for ageostrophic wind fields (vectors, m s^{-1}) and its magnitude (gray scale, m s^{-1}).

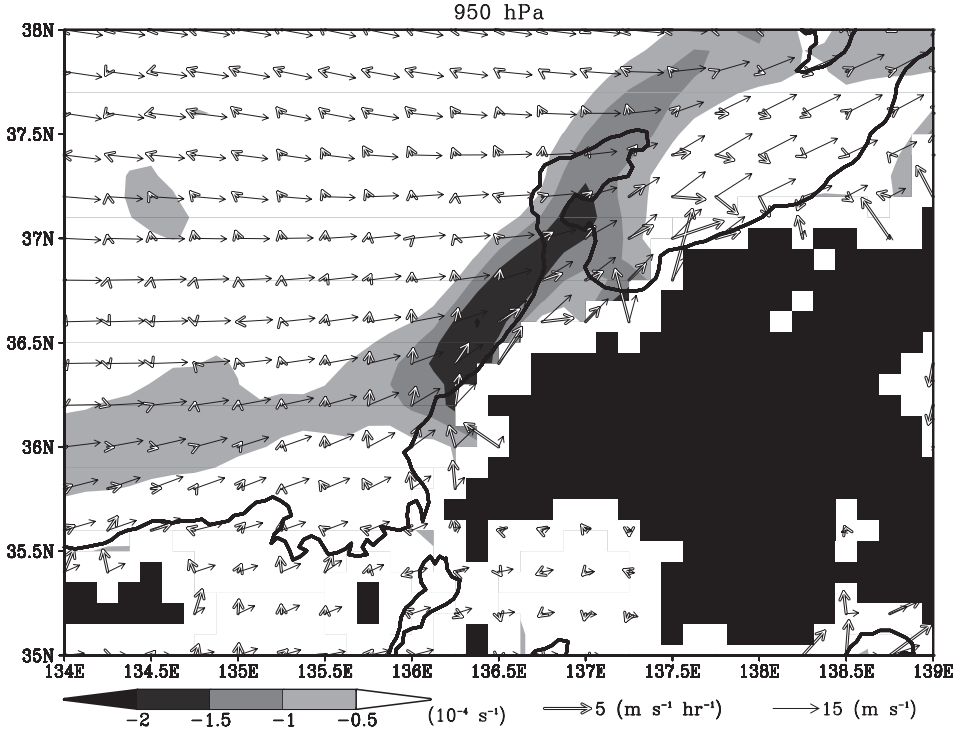

Fig. 13. Coriolis force working on ageostrophic wind (open arrows, m s^{-1} h^{-1}), horizontal wind (solid arrows, m s^{-1}), and horizontal divergence (gray scale, 10^{-4} s^{-1}) at 950 hPa depicted from the MA. All fields were averaged between 0300 JST 25 January 2009 and 0300 JST 27 January 2009.

flank of the Ryohaku Mountains, polarimetric parameters in radar observations are examined. Figure 14 shows the distributions of radar reflectivity Z_h from PPI scans at an elevation angle of 1.9° along the northwest flank of the Ryohaku Mountains. At 0750 JST 25 January 2009 (Fig. 14a), the region enclosed by the ellipse shows a majority of Z_h less than 30 dBZ, although the maximum Z_h is in excess of 35 dBZ. From 0750 JST to 0835 JST (Figs. 14a–d), the moderate reflectivity region forms a line with the maximum Z_h larger than 40 dBZ, and the area with Z_h exceeding 35 dBZ rapidly expands at 0835 JST. After this intensification, the maximum Z_h decreases to approximately 30 dBZ at 0850 JST (Fig. 14e). Such intensification of radar reflectivity was frequently observed in the landfall part of the target cloud band.

PPI displays of ρ_{hv} and K_{DP} at an elevation angle of 1.9° at 0835 JST 25 January, when Z_h becomes maximum (Fig. 14d), are shown in Figs. 15a and 15b, respectively. Z_{DR} is not shown because solid-phase particles in strong reflectivity areas cause significant differential attenuation between horizontal and vertical polarized waves and its correction remains a problem at present. ρ_{hv} is greater than 0.99 for most of the region (Fig. 15a). This indicates dry solid particles, i.e., dry snow and dry graupel are predominant. K_{DP} shows some significant negative values (Fig. 15b). For instance, K_{DP} is less than –0.5° km^{-1} around a 20 km distance north of the radar. This characteristic is different from rain, in case of which K_{DP} shows only zero or positive values.

Figure 16 shows polarimetric parameters averaged between 0300 JST 25 January and 0300 JST 27 January, at an elevation angle of 1.9°. Within a distance of approximately 15 km from the radar site, averaged Z_h is greater than 25 dBZ (Fig. 16a), and on the other hand, ρ_{hv} is smaller than 0.99 on average (Fig. 16b). A distance of 15 km from the radar site at an elevation angle of 1.9° corresponds to a height of 540 m. The larger Z_h and smaller ρ_{hv} is characteristic of melting particles (e.g, Straka et al. 2000). The maximum temperature at the Hakui AMeDAS station, which is located 8.5 km north of the radar site and at 15 m, was 4.8°C between 0300 JST 25 January and 0300 JST 27 January. During the period of higher surface temperature, the hydrometeor type at the surface can be rain. We hereafter focus on microphysical characteristics before the melting of particles and examine the region beyond a distance of 15 km from the radar site. As a result of frequent snowfall intensifications of the target broad cloud band, stronger time-averaged Z_h is present around the coastal region (Fig. 16a). Time-av-

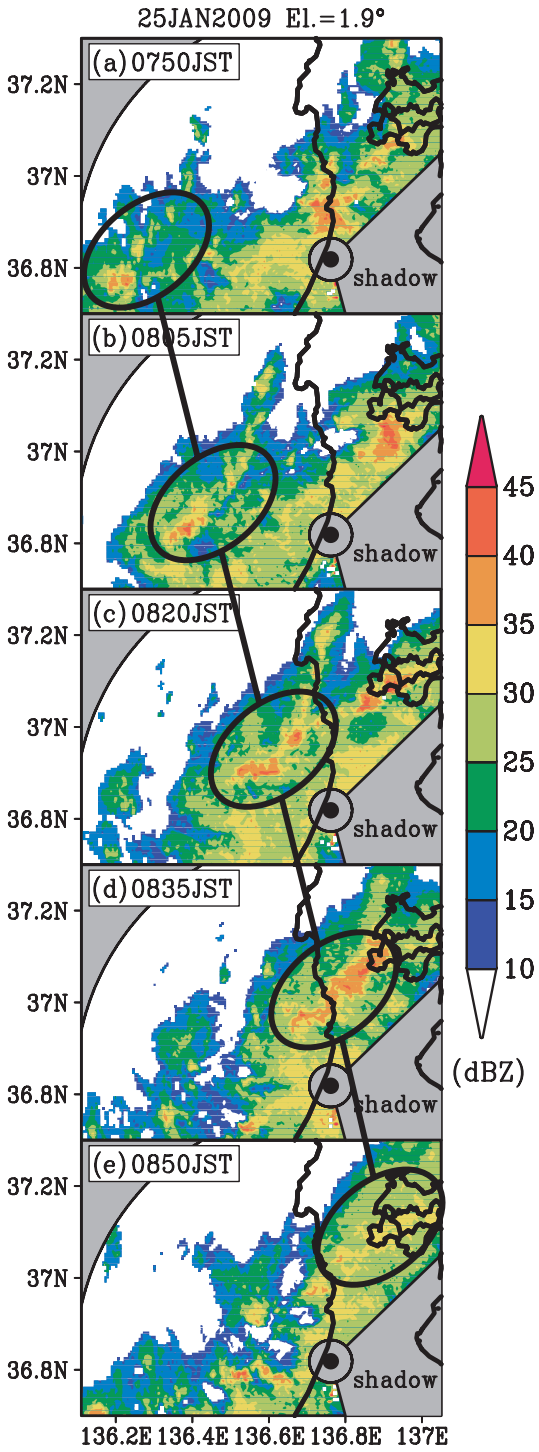

Fig. 14. Radar reflectivity (dBZ) at an elevation angle of 1.9° obtained by a Nagoya University polarimetric radar every 15 min between 0750 JST 25 January 2009 and 0850 JST 25 January 2009. Ellipses indicate regions of intensified radar reflectivity.

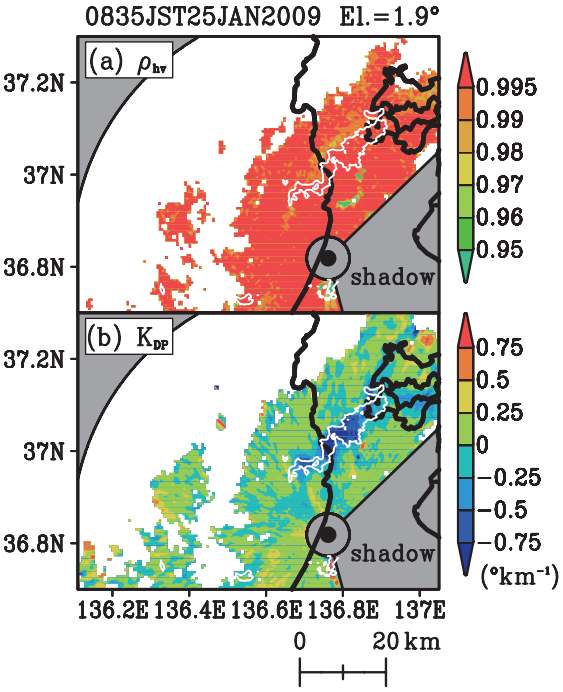

Fig. 15. Polarimetric parameters at an elevation angle of 1.9° obtained by Nagoya University polarimetric radar at 0835 JST 25 January 2009. (a) ρ_{hv} and (b) K_{DP} (° km^{-1}). White contours indicate Z_h of 35 dBZ.

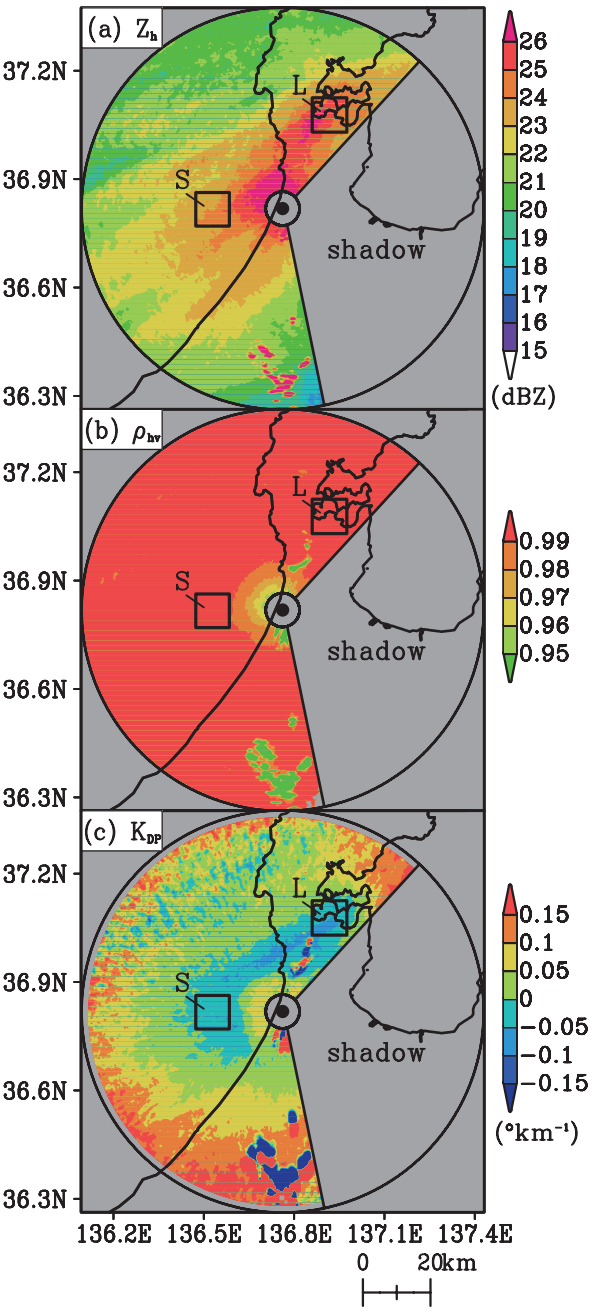

Fig. 16. Time-averaged polarimetric parameters at an elevation angle of 1.9° between 0300 JST 25 January 2009 and 0300 JST 27 January 2009. (a) Z_h (dBZ), (b) ρ_{hv}, and (c) K_{DP} (° km^{-1}).

eraged K_{DP} (Fig. 16c) decreases with the increase in time-averaged Z_h. For regions with time-averaged Z_h larger than 23–24 dBZ, K_{DP} shows negative values on average.

From these polarimetric parameter patterns, 10 km square regions over and around land (Region L in Fig. 16) and over sea (Region S in Fig. 16) corresponding to strong Z_h were selected for the investigation of relative frequency distributions in Z_h–K_{DP} space. The data within the PPI polar coordinate system at an elevation angle of 1.9° were extracted between 0300 JST 25 January and 0300 JST 27 January. Excluding data with weak Z_h (less than 15 dBZ) or low signal-to-noise ratios, 311826 remaining data for Region L and 367739 data for Region S were used to examine relative frequency distributions as the significant echo regions. Most Z_h were below 30 dBZ (Figs. 17a and 17b); relative frequencies of $Z_h < 30$ dBZ were 79% for Region L and 85% for Region S.

In the same square regions, frequencies of scans in which maximum radar reflectivities (Z_{hmax}) exceeding or equal to 35 dBZ or 40 dBZ were calculated. The number of scans was 576 for 48 h (0300 JST 25 January–0300 JST 27 January). The ratios of scans with $Z_{hmax} \geq 35$ dBZ and $Z_{hmax} \geq 40$ dBZ were 35% (31%) and 17% (15%) for Region L (Region S), respectively. It is inferred that the frequently observed high radar

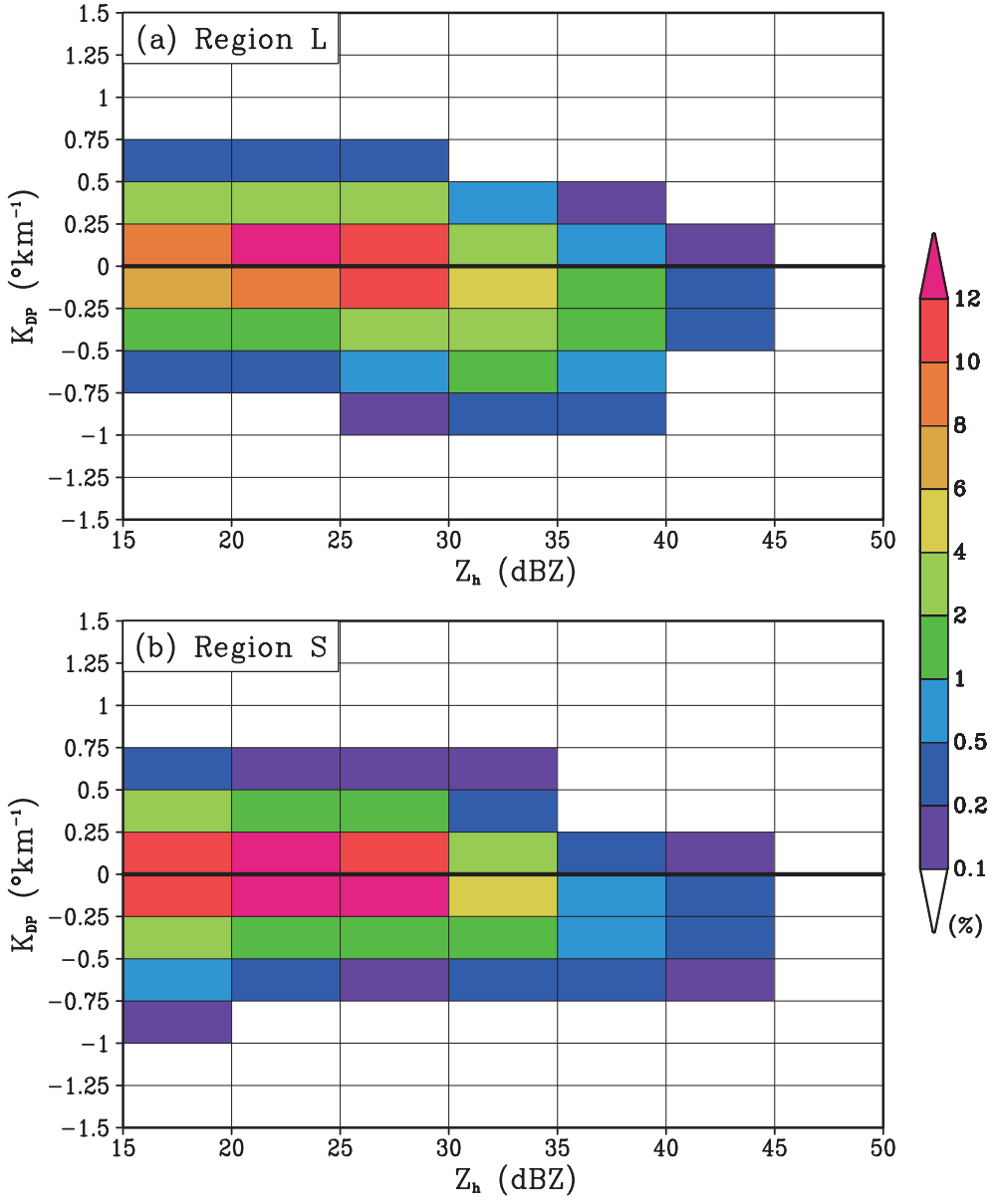

Fig. 17. Relative frequency distributions (%) in Z_h–K_{DP} space, within (a) Region L and (b) Region S shown in Fig. 16 at an elevation angle of 1.9° between 0300 JST 25 January 2009 and 0300 JST 27 January 2009.

reflectivities correspond to the frequent precipitation intensifications.

The modes of K_{DP} are different for lower Z_h and higher Z_h (Figs. 17a and 17b). They have more negative values with increasing Z_h in both Regions L and S. Relative frequency distributions of K_{DP} every 0.25° km^{-1} for $Z_h < 30$ dBZ and $Z_h \geq 30$ dBZ within Region L (Region S) are shown in Figs. 18a (18c) and 18b (18d), respectively. The frequencies have peaks around 0° km^{-1} or with slightly positive values (between 0° km^{-1} and 0.25° km^{-1}) for $Z_h < 30$ dBZ (Figs. 18a and 18c). We discuss the primary hydrometeor type showing this K_{DP} for $Z_h < 30$ dBZ. As hydrometeor types, snow aggregates, graupel, and snow crystals are considered. The absolute values of K_{DP} increase with ice water content (IWC), dielectric constant, and bulk density, while it decreases with axis ratio (vertical/horizontal length ratio) of a hydrometeor particle.

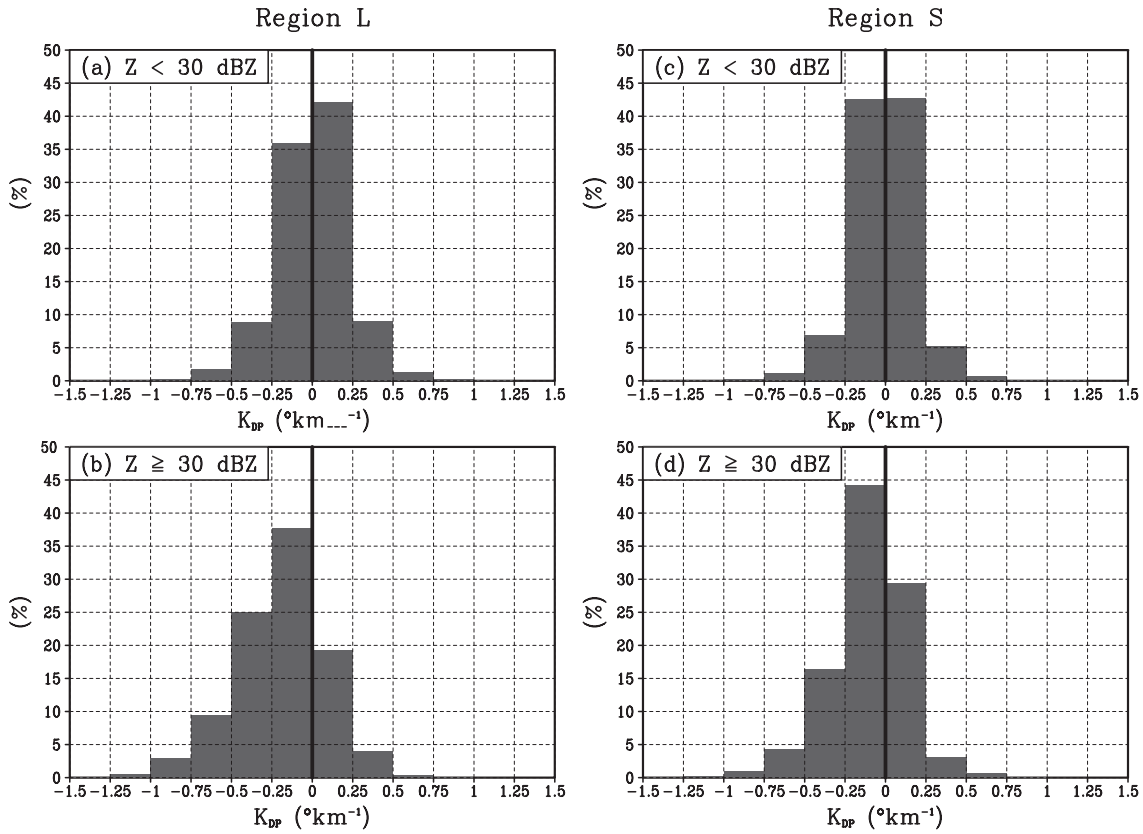

Fig. 18. Relative frequency distributions (%) of K_{DP} for Z_h < 30 dBZ (upper panels) and $Z_h \geq$ 30 dBZ (lower panels) within (a, b) Region L and (c, d) Region S shown in Fig. 16 at an elevation angle of 1.9° between 0300 JST 25 January 2009 and 0300 JST 27 January 2009.

Dielectric constant is larger for wet particles than for dry particles. We suppose that IWC is small for Z_h < 30 dBZ. ρ_{hv} indicates that particle surface is dry at the radar beam height within both Regions L and S. For Z_h < 30 dBZ, snow aggregates show K_{DP} around 0° km^{-1} because of low bulk density (e.g., Carey et al. 2009). Graupel does not show such small axis ratios and gives K_{DP} around 0° km^{-1}. Snow crystals with axis ratios near unity (spherical particles) also show K_{DP} around 0° km^{-1}. Only snow crystals with small axis ratios (flat snow crystals) can produce large K_{DP} corresponding to 0.5–2° km^{-1} in X-band radar observations (e.g., Kennedy and Rutledge 2011), where it should be noted that K_{DP} is proportional to the inverse of radar wavelength, as shown in Bringi and Chandrasekar (2001). Therefore, shapes and hydrometeor types are unclear in the region of K_{DP} near 0° km^{-1} for Z_h < 30 dBZ, while flat snow crystals with significantly positive K_{DP} (0.5–2° km^{-1}) are not the primary particle type in the present case.

For $Z_h \geq$ 30 dBZ (Figs. 18b and 18d), in comparison with the distribution for Z_h < 30 dBZ, frequencies of K_{DP} less than –0.25° km^{-1} (K_{DP} greater than or equal to 0° km^{-1}) are higher (lower). The modes of K_{DP} for $Z_h \geq$ 30 dBZ have peaks between –0.25° km^{-1} and 0° km^{-1} in both Regions L and S. This reveals that vertically oriented particles are predominant for $Z_h \geq$ 30 dBZ. According to Straka et al. (2000) and Dolan and Rutledge (2009), vertically oriented particles with moderate-to-strong Z_h are prolate graupel and their shape appears conical. At the radar site, several close-up photographs of precipitation particles were taken. Conical graupel particles were seen in a few photographs; however, these could not be compared to K_{DP} because of the unavailability of data within a distance of 4.8 km from the radar.

The characteristics of polarimetric parameters are summarized as follows. Above melting levels, flat snow crystals were not a primary particle type for Z_h < 30 dBZ. When snowfall intensified ($Z_h \geq 30$ dBZ), frequencies of prolate graupel increased as a primary particle. In some periods and/or regions of surface temperature above 0°C, the hydrometeors were melting particles or possibly rain particles.

6. Discussion of intensification along the mountain flank

During the life of the target broad cloud band, surface lows and a trough over the central Sea of Japan maintained the predominant westerly winds over the southern part of the sea, around the San-in and Hokuriku regions. These westerlies were blocked by the Ryohaku Mountains, and a local high-pressure region formed upwind of the mountains. When nearly geostrophic flow entered such a high pressure region, there yielded an imbalance between the pressure gradient and the Coriolis forces. The unbalanced flow was forced toward the left in the high-pressure region, which formed winds with a southerly component. Ookubo and Kurokawa (2000) and Yoshihara et al. (2004) showed that flows deflected by mountains generated heavy snowfall or snowfall intensification during cold-air outbreaks. In their studies, surrounding winds were deflected toward the left in the upwind of mountains and made convergence with the non-deflected flow. The similar characteristic was also found in the present case. The present study showed the reasonability of deflection by using non-dimensional mountain height and demonstrated the dynamics of deflection.

Houze (2012) showed a blocking effect of a two-dimensional mountain on precipitation (Fig. 19a). Suppose that the two-dimensional mountain in Fig. 19a extends infinitely into and out of the page. When an air upstream of the mountain has large non-dimensional mountain height (stable and/or weak cross-mountain flow), the air tends to pile up instead of rising over the terrain. He explained that the effect of mountain range is shifted upstream and the air is lifted ahead of the mountain, which forms cloud and precipitation. In the two-dimensional mountain case, a two-dimensional convergence line should form upwind of the mountain range. On the other hand, the shape of the Ryohaku Mountains that contributed to the flow deflection is isolated rather than two dimensional. Airflow around the mountains and intensification of snowfall are schematically shown in Fig. 19b. The blocking of environmental flow upstream of the mountains deflects

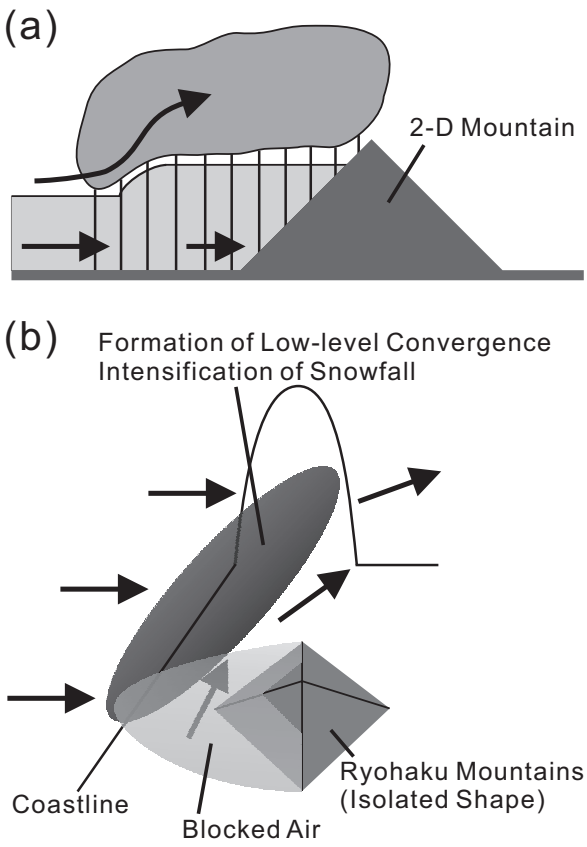

Fig. 19. (a) Blocking effect of a two-dimensional mountain (extending infinitely into and out of the page) on precipitation (Houze 2012). (b) Blocking and deflection of airflow upstream of the Ryohaku mountains and intensification process of snowfall along the mountain flank, which is shown in this study. Straight arrows represent low-level flows.

low-level flow to the left-hand side. The deflected winds make a convergence with the environmental flow. On the other hand, the environmental flow north of the mountains is affected little by the mountains. Therefore, the convergence between environmental flow and deflected flow did not have a structure of a long line, but was localized along the mountain flank.

Preexisting precipitation echoes moving along the target broad cloud band were intensified in the local low-level convergence formed along the mountain flank. Intensifications of preexisting precipitation echoes during cold-air outbreaks have also been shown in Tsuboki et al. (1989) and Yoshihara et al. (2004). The low-level convergence formed along mountain flanks enhances updraft associated with preexisting echoes.

The enhanced updraft forms a large amount of cloud particles. Solid precipitation particles in the preexisting echoes collect the cloud particles formed in the intensified updraft to become graupel efficiently. This process would frequently produce vertically oriented graupel showing characteristic negative K_{DP}.

Figure 20 shows a relation between upper-level (500 hPa) temperature (T_{500}; Fig. 20a) and $\hat{h}$ for a mountain height of 2702 m (Fig. 20b) in January 2009, derived from upper-air sounding observations at Wajima. When cold air is present at the upper level, the $\hat{h}$ values tend to decrease because the development of convective mixing layer destabilizes the stratification to be closer to neutral at the low level. The averaged critical levels, where $\hat{h}$ equals unity, (bold line in Fig. 20b) are 1360 m (standard deviation: 409 m) for $T_{500} < -30$°C and 1870 m (standard deviation: 364 m) for $T_{500} > -30$°C. However, even when upper-level cold air is present over the Sea of Japan, the blocking and deflection of airflow frequently occur below heights of approximately 1000 m in areas upwind of mountains of 2500–3000 m elevations in central Japan, such as the Ryohaku and Hida Mountains. It is inferred that this blocking and deflection of airflow contribute to snowfall intensifications around coastal regions along the upwind side or flanks of high mountains.

7. Summary

A broad cloud band formed along the northern coastal region of western Japan and persisted for approximately 2 days from 25 to 27 January, 2009, during a cold-air outbreak. In the band, snowfall was remarkably intensified along the flank of a high mountain region in central Japan. A precipitation maximum of 95.5 mm for the 2 days was observed in the intensified precipitation region. The intensification caused local concentration of substantial precipitation. To understand this concentration, we studied dynamical processes causing snowfall intensification and microphysical characteristics of the intensified region.

During the lifetime of the broad cloud band under cold-air outbreak conditions, two low-pressure systems formed successively over the central Sea of Japan, which moved eastward. After the second low passed the Japanese Islands, a weak east–west trough formed over the central part of the sea. When the cyclones and the trough were present over the Sea of Japan, isobars over the southwest part of the sea were oriented in the east–west direction, producing predominant westerlies in that area. To the south of the broad cloud band, predominant surface winds were southerly over the land. The southerly winds produced a convergence zone corresponding to the target cloud band.

To the south of the intensified precipitation region, southwesterly winds with high DC were present from the Kanazawa Plain to the Noto Peninsula. High DC indicates that the localized southwesterlies were maintained under the predominant westerlies. Low-level geopotential height fields depicted from the objective analysis data showed that a local high-pressure gradient was present upwind of high mountain regions. The forces derived from the height and wind fields showed a large imbalance over the high-pressure-gradient region, which produced ageostrophic winds. Consequently, air from the west into the high-pressure-gradient region encountered forcing toward the left, generating winds with a southerly component. The non-dimensional mountain height $\hat{h}$ showed that airflow at least below 900 m was blocked by the Ryohaku Mountains. Eventually, this blocking generated the local high-pressure region that in turn formed the southwesterlies. These southwesterlies then caused a wind convergence along the mountain flank, which amplified snowfall amounts. In this study, the formation of high-pressure region upstream of the Ryohaku Mountains was explained by a dynamical contribution associated with the blocking of mountains. A quantitative contribution of thermodynamic processes such as land–sea surface heating contrast remains to be studied.

In addition, precipitation intensification processes of the broad cloud band were examined using the X-band polarimetric radar of Nagoya University, placed at Oshimizu in Hokuriku. The ratios of radar observation grids with $Z_h < 30$ dBZ and $Z_h \geq 30$ dBZ were 79% (85%) and 21% (15%), respectively, within the time-averaged significant echo region in Region L (Region S) shown in Fig. 16 for 2 days (0300 JST 25 Janaury–0300 JST 27 January). In Region L (Region S), the total times in which the maximum Z_h exceeded or equaled 35 and 40 dBZ were 35% (31%) and 17% (15%) of the 2 days, respectively. ρ_{hv} averaged for the 2 days was lower than 0.99 below a height of several hundred meters. The low time-averaged ρ_{hv} and surface temperatures indicate that melting particles were present at the lowest level in some periods and/or regions of surface temperature above 0°C. Above melting levels, K_{DP} occasionally showed negative values, less than –0.5° km^{-1}. The frequency distributions of K_{DP} showed significantly negative values for $Z_h \geq 30$ dBZ, in contrast to a peak of K_{DP} around 0° km^{-1} for $Z_h < 30$ dBZ. These polarimetric parameters indicate that vertically oriented graupel, which could be conical, increased as a primary particle with increasing Z_h in the intensified precipitation region of

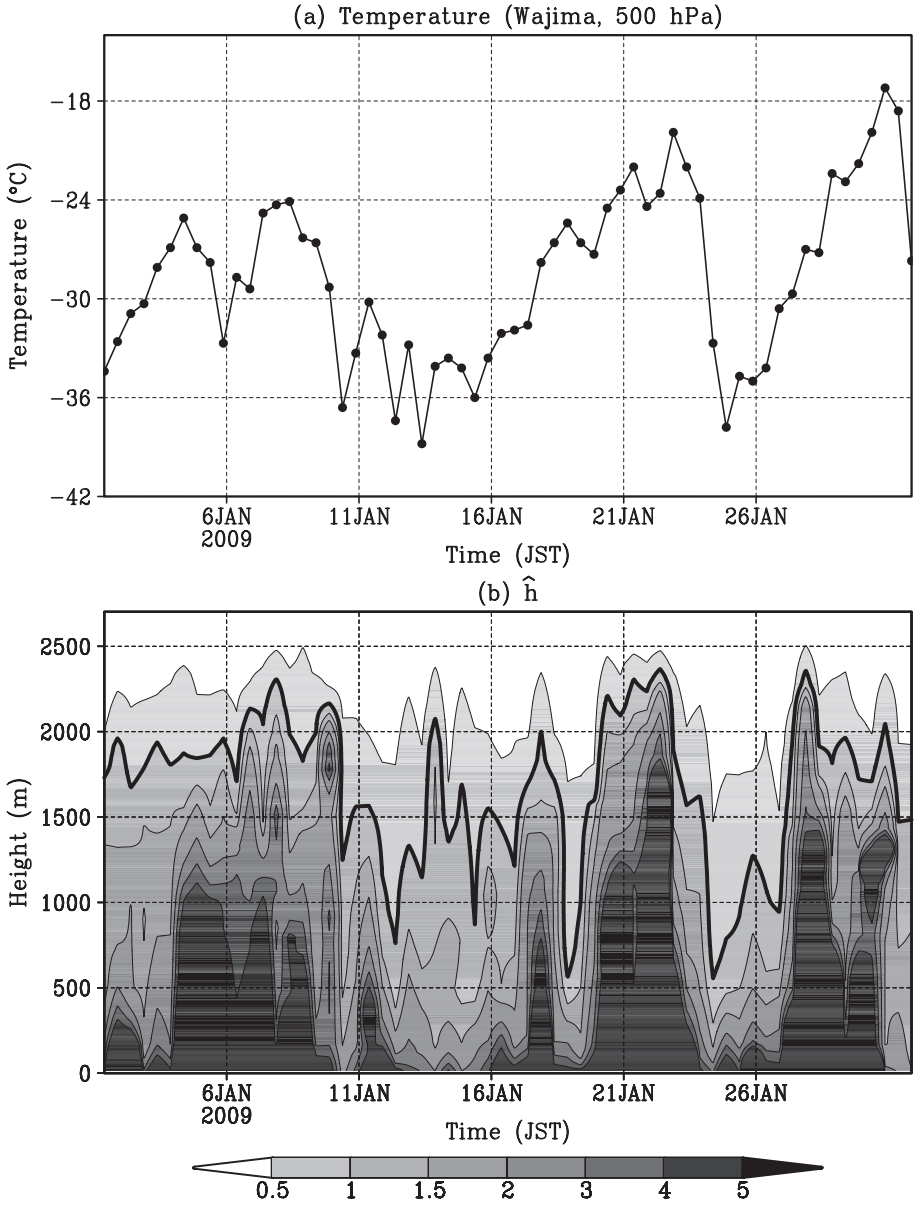

Fig. 20. (a) Temperature at 500 hPa and (b) non-dimensional mountain heights ($\hat{h}$) for a mountain height of 2702 m in January 2009 derived from upper-air sounding observations at Wajima. A thick contour in (b) is a line where values of non-dimensional mountain height $\hat{h}$ equal unity.

the cloud band.

Caylor and Chandrasekar (1996) and Carey and Rutledge (1998) showed that small snow crystals, less than 1–2 mm, may be vertically aligned within vertical strong electric fields associated with lightning discharges and produce negative K_{DP}. Based on theoretical simulations, Carey et al. (2009) showed that when prolate graupel coexist with vertically oriented snow crystals, the negative K_{DP} produced by the graupel is enhanced by the crystals. In the present study, frequent thunders were confirmed near the intensified precipitation region. Therefore, the possibility where vertically oriented snow crystals contribute to negative K_{DP} should be examined in our future work.

We explained the reasonability of flow deflection by high mountains and its dynamics. In addition,

it was inferred that deflection of airflow frequently occurs upwind of the central mountains of Japan (with heights of 2500–3000 m) during cold-air outbreaks and contributes to snowfall intensifications around the coastal regions along the upwind sides or flanks of high mountains.

Although the present study clarified the observed characteristics of the broad cloud band and the precipitation intensification processes along the flank of a high mountain region, the formation mechanism of the target broad cloud band remains to be studied. Climatologies of environmental conditions and formation frequency of such a broad cloud band should also be investigated in our future work.

Acknowledgments

We express our thanks to Prof. K. Muramoto and Dr. M. Kubo of Kanazawa University and Mr. K. Chikaoka of the Hodatsushimizu Town Hall for their cooperation in radar observation at Hokuriku. We are also grateful to Dr. H. Minda of Nagoya University for his help with the radar installation, and Dr. S. Endo, Dr. M. Oue, Mr. H. Okamoto, and Mr. T. Kouketsu of Nagoya University for helping with radar operation and maintenance. Thanks are extended to the editor, Dr. T. Kato, and reviewers for their comments, which greatly contributed to improving the manuscript. This study was jointly supported by a Grant-in-Aid for Young Scientists B (20740271 and 24740319) of the Ministry of Education, Culture, Sports, Science and Technology of Japan, and the "Virtual Laboratory for the Earth's Climate Diagnostics" program.

References

Asai, T., 1988: Meso-scale features of heavy snowfalls in Japan Sea coastal regions of Japan. *Tenki*, **35**, 156–161 (in Japanese).

Atkinson, B. W., and J. W. Zhang, 1996: Mesoscale shallow convection in the atmosphere. *Rev. Geophys.*, **34**, 403–431.

Bringi, V. N., and V. Chandrasekar, 2001: *Polarimetric Doppler Weather Radar: Principles and Applications*. Cambridge University Press, 636 pp.

Bromwich, D. H., 1989: An extraordinary katabatic wind regime at Terra Nova Bay, Antarctica. *Mon. Wea. Rev.*, **117**, 688–695.

Brown, R. A., 1980: Longitudinal instabilities and secondary flows in the planetary boundary layer: A review. *Rev. Geophys. Space Phys.*, **18**, 683–697.

Carey, L. D., W. A. Petersen, and W. K. Deierling, 2009: Radar differential phase signatures of ice orientation for the prediction of lightning initiation and cessation. *Proc. 34th Conf. on Radar Meteor.*, 13 pp.

Carey, L. D., and S. A. Rutledge, 1998: Electrical and multiparameter radar observations of a severe hailstorm. *J. Geophys. Res.*, **103**, 13979–14000.

Caylor, I. J., and V. Chandrasekar, 1996: Time-varying ice crystal orientation in thunderstorms observed with multiparameter radar. *IEEE Trans. Geosci. Remote Sens.*, **34**, 847–858.

Dolan, B., and S. A. Rutledge, 2009: A theory-based hydrometeor identification algorithm for X-band polarimetric radars. *J. Atmos. Oceanic Technol.*, **26**, 2071–2088.

Eito, H., T. Kato, M. Yoshizaki, and A. Adachi, 2005: Numerical simulation of the quasi-stationary snowband observed over the southern coastal area of the Sea of Japan on 16 January 2001. *J. Meteor. Soc. Japan*, **83**, 551–576.

Eito, H., M. Murakami, C. Muroi, T. Kato, S. Hayashi, H. Kuroiwa, and M. Yoshizaki, 2010: The structure and formation mechanism of transversal cloud bands associated with the Japan-Sea Polar-Airmass Convergence Zone. *J. Meteor. Soc. Japan*, **88**, 625–648.

Etling, D., and R. A. Brown, 1993: Roll vortices in the planetary boundary layer: A review. *Bound.-Layer Meteor.*, **65**, 215–248.

Fujiyoshi, Y., M. Kawashima, M. Ohi, C. Fujiwara, T. Kamisho, and K. Mukasa, 2009: Radar echo properties of a broad cloud band formed on the shores of the Sea of Okhotsk. *Proceedings of the Spring Meeting of the Meteorological Society of Japan 2009,* Meteor. Soc. Japan, 374 (in Japanese).

Fujiyoshi, Y., K. Tsuboki, H. Konishi, and W. Gorow, 1988: Doppler radar observation of convergence band cloud formed on the west coast of Hokkaido Island (I) -Warm fontal type-. *Tenki*, **35**, 427–439 (in Japanese).

Fujiyoshi, Y., K. Tsuboki, S. Satoh, and G. Wakahama, 1992: Three-dimensional radar echo structure of a snow band formed on the lee side of a mountain. *J. Meteor. Soc. Japan*, **70**, 11–24.

Fujiyoshi, Y., N. Yoshimoto, and T. Takeda, 1998: A dual-Doppler radar study of longitudinal-mode snowbands. Part I: A three-dimensional kinematic structure of meso-γ-scale convective cloud systems within a longitudinal-mode snowband. *Mon. Wea. Rev.*, **126**, 72–91.

Grim, J. A., N. F. Laird, and D. A. R. Kristovich, 2004: Mesoscale vortices embedded within a lake-effect shoreline band. *Mon. Wea. Rev.*, **132**, 2269–2274.

Hjelmfelt, M. R., 1990: Numerical study of the influence of environmental conditions on lake-effect snowstorms over Lake Michigan. *Mon. Wea. Rev.*, **118**, 138–150.

Houze Jr., R. A., 2012: Orographic effects on precipitating clouds. *Rev. Geophys.*, **50**, RG1001, doi:10.1029/2011RG000365.

Ino, H., 1965: A discontinuity line formed over Wakasa Bay in winter. *Meteor. Res. Note*, **16**, 329–332 (in Japanese).

Ishihara, M., H. Sakakibara, and Z. Yanagisawa, 1989: Doppler radar analysis of the structure of mesoscale snow bands developed between the winter monsoon and the land breeze. *J. Meteor. Soc. Japan*, **67**, 503–520.

Japan Meteorological Agency, 1968: Heavy snowfalls in the Hokuriku district. *Technical Report of the Japan Meteorological Agency*, **66**, 481 pp (in Japanese).

Katsutani, M., 1947: Discontinuity line generated in winter monsoon and snowfall on the Sea of Japan side. *Kenkyu Sokuho of the Central Meteorological Observatory of Japan*, **28**, 1–9 (in Japanese).

Kawase, H., T. Sato, and F. Kimura, 2005: Numerical experiments on cloud streets in the lee of island arcs during cold-air outbreaks. *Geophys. Res. Lett.*, **32**, L14823, doi:10.1029/2005GL023256.

Kennedy, P. C., and S. A. Rutledge, 2011: S-band dual-polarization radar observations of winter storms. *J. Appl. Meteor. Climatol.*, **50**, 844–858.

Kuettner, J., 1959: The band structure of the atmosphere. *Tellus*, **11**, 267–294.

Kuettner, J. P., 1971: Cloud bands in the earth's atmosphere: Observations and theory. *Tellus*, **23**, 404–426.

Laird, N. F., J. E. Walsh, and D. A. R. Kristovich, 2003: Model simulations examining the relationship of lake-effect morphology to lake shape, wind direction, and wind speed. *Mon. Wea. Rev.*, **13**, 2102–2111.

Liu, A. Q., G. W. K. Moore, K. Tsuboki, and I. A. Renfrew, 2004: A high-resolution simulation of convective roll clouds during a cold-air outbreak. *Geophys. Res. Lett.*, **31**, L03101, doi:10.1029/2003GL018530.

Maesaka, T., G. W. K. Moore, Q. Liu, and K. Tsuboki, 2006: A simulation of a lake effect snowstorm with a cloud resolving numerical model. *Geophys. Res. Lett.*, **33**, L20813, doi:10.1029/2006GL026638.

Markowski, P., and Y. Richardson, 2010: *Mesoscale Meteorology in Midlatitudes*. Wiley, 430 pp.

Morotomi, K., T. Shinoda, Y. Shusse, T. Kouketsu, T. Ohigashi, K. Tsuboki, H. Uyeda, and I. Tamagawa, 2012: Maintenance mechanisms of a precipitation band formed along the Ibuki-Suzuka Mountains on September 2–3, 2008. *J. Meteor. Soc. Japan*, **90**, 737–753.

Muramatsu, T., 1979: The cloud line enhanced by upwind orographic features in winter monsoon situations. *Geophys. Mag.*, **38**, 1–15.

Nagata, M., 1987: On the structure of a convergent cloud band over the Japan Sea in winter; a prediction experiment. *J. Meteor. Soc. Japan*, **65**, 871–883.

Nagata, M., 1991: Further numerical study on the formation of the convergent cloud band over the Japan Sea in winter. *J. Meteor. Soc. Japan*, **69**, 419–428.

Nagata, M., 1992: Modeling case study of the Japan-Sea convergent cloud band in a varying large-scale environment: Evolution and upscale effect. *J. Meteor. Soc. Japan*, **70**, 649–671.

Nagata, M., M. Ikawa, S. Yoshizumi, and T. Yoshida, 1986: On the formation of a convergent cloud band over the Japan Sea in winter; numerical experiments. *J. Meteor. Soc. Japan*, **64**, 841–855.

Ninomiya, K., 1989: Polar/comma-cloud lows over the Japan Sea and the northwestern Pacific in winter. *J. Meteor. Soc. Japan*, **67**, 83–97.

Niziol, T. A., W. R. Snyder, and J. S. Waldstreicher, 1995: Winter weather forecasting throughout the eastern United States. Part IV: Lake effect snow. *Wea. Forecasting*, **10**, 61–77.

Ohigashi, T., and K. Tsuboki, 2005: Structure and maintenance process of stationary double snowbands along the coastal region. *J. Meteor. Soc. Japan*, **83**, 331–349.

Ohigashi, T., and K. Tsuboki, 2007: Shift and intensification processes of the Japan-Sea polar-airmass convergence zone associated with the passage of a mid-tropospheric cold core. *J. Meteor. Soc. Japan*, **85**, 633–662.

Ohigashi, T., K. Tsuboki, and S. Ishizuka, 2012: Structure of a snowband formed in the southern edge of a decaying broad cloud band over the Sea of Japan. *Tenki*, **59**, 33–46 (in Japanese).

Ohtake, H., M. Kawashima, and Y. Fujiyoshi, 2009: The formation mechanism of a thick cloud band over the northern part of the Sea of Japan during cold air outbreaks. *J. Meteor. Soc. Japan*, **87**, 289–306.

Okabayashi, T., 1969: Photograph of heavy snowfall on Japan Seaside on Jan. 2 1969, taken by ESSA. *Tenki*, **16**, 79–80 (in Japanese).

Onogi, K., J. Tsutsui, H. Koide, M. Sakamoto, S. Kobayashi, H. Hatsushika, T. Matsumoto, N. Yamazaki, H. Kamahori, K. Takahashi, S. Kadokura, K. Wada, K. Kato, R. Oyama, T. Ose, N. Mannoji, and R. Taira, 2007: The JRA-25 reanalysis. *J. Meteor. Soc. Japan*, **85**, 369–432.

Ookubo, A., and Y. Kurokawa, 2000: Structure of shear line with heavy snowfall and with low visibility formed in Toyama Prefecture in a case of winter conditions. *Tenki*, **47**, 255–266 (in Japanese).

Orlanski, I., 1975: A rational subdivision of scales for atmospheric processes. *Bull. Amer. Meteor. Soc.*, **56**, 527–530.

Passarelli Jr., R. E., and R. R. Braham Jr., 1981: The role of the winter land breeze in the formation of great lake snow storms. *Bull. Amer. Meteor. Soc.*, **62**, 482–491.

Rasmussen, E. A., and J. Turner (eds.), 2003: *Polar Lows*. Cambridge University Press, 612 pp.

Renfrew, I. A., and G. W. K. Moore, 1999: An extreme cold-air outbreak over the Labrador Sea: Roll vortices and air-sea interaction. *Mon. Wea. Rev.*, **127**, 2379–2394.

Sasaki, H., and T. Satomura, 1991: Numerical experiments on convergence cloud bands over the northern part of the Japan Sea. *J. Meteor. Soc. Japan*, **69**, 375–388.

Schuur, T., A. Ryzhkov, and P. Heinselman, 2003: *Observations and classification of echoes with the polarimetric*

WSR-88D radar. National Severe Storms Laboratory Rep., 46 pp.

Shusse, Y., K. Nakagawa, N. Takahashi, S. Satoh, and T. Iguchi, 2009: Characteristics of polarimetric radar variables in three types of rainfalls in a baiu front event over the East China Sea. *J. Meteor. Soc. Japan*, **87**, 865–875.

Straka, J. M., D. S. Zrnic, and A. V. Ryzhkov, 2000: Bulk hydrometeor classification and quantification using polarimetric radar data: Synthesis of relations. *J. Appl. Meteor.*, **39**, 1341–1372.

Takeda, T., K. Isono, M. Wada, Y. Ishizaka, K. Okada, Y. Fujiyoshi, M. Maruyama, Y. Izawa, and K. Nagaya, 1982: Modification of convective snow-clouds in landing the Japan Sea coastal region. *J. Meteor. Soc. Japan*, **60**, 967–977.

Tsuboki, K., Y. Fujiyoshi, and G. Wakahama, 1989a: Doppler radar observation of convergence band cloud formed on the west coast of Hokkaido Island. II: Cold frontal type. *J. Meteor. Soc. Japan*, **67**, 985–999.

Tsuboki, K., Y. Fujiyoshi, and G. Wakahama, 1989b: Structure of a land breeze and snowfall enhancement at the leading edge. *J. Meteor. Soc. Japan*, **67**, 757–770.

Yagi, S., T. Muramatsu, T. Uchiyama, and N. Kurokawa, 1986: "Convergent band cloud" and "Cu-Cb line" over the Japan Sea affected by topographic features in the coast of the Asian Continent. *Tenki*, **33**, 453–465 (in Japanese).

Yamada, Y., M. Murakami, H. Mizuno, M. Maki, S. Nakai, and K. Iwanami, 2010: Kinematic and thermodynamical structures of longitudinal-mode snow bands over the Sea of Japan during cold-air outbreaks Part I: Snow bands in large vertical shear environment in the band-transverse direction. *J. Meteor. Soc. Japan*, **88**, 673–718.

Yanase, W., and H. Niino, 2007: Dependence of polar low development on baroclinicity and physical processes: An idealized high-resolution numerical experiment. *J. Atmos. Sci.*, **64**, 3044–3067.

Yoshihara, H., M. Kawashima, K. Arai, J. Inoue, and Y. Fujiyoshi, 2004: Doppler radar study on the successive development of snowbands at a convergent line near the coastal region of Hokuriku district. *J. Meteor. Soc. Japan*, **82**, 1057–1079.

Yoshimoto, N., Y. Fujiyoshi, and T. Takeda, 2000: A dual-Doppler radar study of longitudinal-mode snowbands Part II: Influence of the kinematics of a longitudinal-mode snowband on the development of an adjacent snowband. *J. Meteor. Soc. Japan*, **78**, 381–403.

Young, G. S., D. A. R. Kristovich, M. R. Hjelmfelt, and R. C. Foster, 2002: Rolls, streets, waves, and more: A review of quasi-two-dimensional structures in the atmospheric boundary layer. *Bull. Amer. Meteor. Soc.*, **83**, 997–1001.